# The Alzheimer's gene *SORL1* is a regulator of endosomal traffic and recycling in human neurons

Swati Mishra[1,2*], Allison Knupp[1,2*], Marcell P. Szabo[1,2], Charles A. Williams[1,2], Chizuru Kinoshita[1,2], Dale W. Hailey[1,2], Yuliang Wang[2,3], and Jessica E. Young[1,2,#]

[1]Department of Laboratory Medicine and Pathology

[2]Institute for Stem Cell and Regenerative Medicine

[3]School of Computer Science and Engineering

University of Washington Seattle WA, 98195, USA

[#]Correspondence: jeyoung@uw.edu

[*]Equal Contribution

Author emails: swatim2@uw.edu, knuppa@uw.edu, szabom@uw.edu, cwil@uw.edu ckino@uw.edu, dhailey@uw.edu, yuliangw@uw.edu, jeyoung@uw.edu

## ABSTRACT

**Background** Loss of the Sortilin-related receptor 1 (*SORL1*) gene seems to act as a causal event for Alzheimer's disease (AD). Recent studies have established that loss of *SORL1*, as well as mutations in autosomal dominant AD genes *APP* and *PSEN1/2*, pathogenically converge by swelling early endosomes, AD's cytopathological hallmark. Acting together with the retromer trafficking complex, *SORL1* has been shown to regulate the recycling of the amyloid precursor protein (APP) out of the endosome, contributing to endosomal swelling and to APP misprocessing. We hypothesized that *SORL1* plays a broader role in neuronal endosomal recycling and used human induced pluripotent stem cell derived neurons (hiPSC-Ns) to test this hypothesis. We examined endosomal recycling of three transmembrane proteins linked to AD pathophysiology: APP, the BDNF receptor Tropomyosin-related kinase B (TRKB), and the glutamate receptor subunit AMPA1 (GLUA1).

**Methods** We used isogenic hiPSCs engineered to have *SORL1* depleted or to have enhanced *SORL1* expression. We differentiated neurons from these cell lines and mapped the trafficking of APP, TRKB and GLUA1 within the endosomal network using confocal microscopy. We also performed cell surface recycling and lysosomal degradation assays to assess the functionality of the endosomal network in both *SORL1* depleted and overexpressing neurons. Finally, we analyzed alterations in gene expression in *SORL1* depleted neurons using RNA-sequencing.

**Results** We find that as with APP, endosomal trafficking of GLUA1 and TRKB is impaired by loss of *SORL1*. We show that trafficking of all three cargo to late endosomes and lysosomes is affected by manipulating SORL1 expression. We also show that depletion of *SORL1* significantly impacts the endosomal recycling pathway for APP and GLUA1 at the level of the recycling endosome and trafficking to the cell surface. This has a functional effect on neuronal activity as shown by multi-electrode array (MEA). Conversely, increased *SORL1* expression enhances endosomal recycling for APP and GLUA1. Our unbiased transcriptomic data further support *SORL1*'s role in endosomal recycling. We observe altered expression networks that regulate cell surface trafficking and neurotrophic signaling in SORL1 depleted neurons.

**Conclusion** Collectively, and together with other recent observations, these findings suggest that *SORL1* is a broad regulator of retromer-dependent endosomal recycling in neurons, a conclusion that has both pathogenic and therapeutic implications for Alzheimer's disease.

**KEY WORDS**

Human induced pluripotent stem cells, neurons, Alzheimer's disease, endosomal network, *SORL1*.

## BACKGROUND

52 Alzheimer's disease (AD) is a progressive neurodegenerative disorder and the most common
53 cause of dementia. The underlying contributors to AD pathology encompass several biological
54 pathways, including endosomal function, amyloid precursor protein (APP) processing, immune
55 function, synaptic function, and lipid metabolism(Karch and Goate, 2015). Among these,
56 endosomal dysfunction in neurons is emerging as a potential causal mechanism(Small and
57 Petsko, 2020). Mutations in the amyloid precursor protein (*APP*) and the two presenilins (*PSEN1*
58 and *PSEN2*) lead to early-onset autosomal dominant AD. When these mutations are modelled in
59 human neurons and other systems they cause endosomal swelling, indicative of traffic jams, a
60 phenotype that is a cytopathological hallmark of AD(Cataldo et al., 2000; Choi et al., 2013; Kwart
61 et al., 2019). Recent genetic studies have identified a fourth gene, the trafficking receptor 'sortilin
62 related receptor 1' (*SORL1*), which, when harboring frame-shift mutations leading to premature
63 stop codons, is described as causal for AD(Holstege et al., 2017; Raghavan et al., 2018;
64 Scheltens et al., 2021). Interestingly, *SORL1* is also linked to the more common, late-onset form
65 of AD(Lambert et al., 2013; Rogaeva et al., 2007b) and its expression is lost in sporadic AD brains
66 (Dodson et al., 2006; Thonberg et al., 2017). When modelled in human neurons, *SORL1* depletion
67 phenocopies *APP* and *PSEN* mutations by causing endosomal swelling(Hung et al., 2021; Knupp
68 et al., 2020).
69
70 The *SORL1* gene codes for the protein SORLA, an endosomal sorting protein that is also an
71 adaptor molecule for the retromer trafficking complex (Fjorback et al., 2012; Rogaeva et al.,
72 2007a; Small and Gandy, 2006). Retromer recycles cargo out of the early endosome, either from
73 the endosome to the trans-Golgi network or, with greater importance for neurons, back to the cell
74 surface(Fjorback et al., 2012; Seaman, 2012). To date, the best evidence for *SORL1*'s role in
75 retromer-dependent endosomal recycling comes from studies investigating APP
76 trafficking(Fjorback et al., 2012; Schmidt et al., 2007; Willnow and Andersen, 2013). Our previous

77 work demonstrated that *SORL1* depletion retains APP in early endosomes, which may contribute
78 to endosomal swelling by blocking recycling(Knupp et al., 2020).
79
80 Retromer-dependent trafficking in neurons, however, also recycles cargo other than APP. For
81 example, retromer is required for the normal recycling of glutamate receptors, a trafficking event
82 that mediates synaptic plasticity and synaptic health, and this dependency occurs independent of
83 retromer's role in APP recycling(Park et al., 2004; Temkin et al., 2017). Neurotrophin receptors
84 are also trafficked through the endosomal system, in a retromer-dependent manner, and are
85 important for synaptic health(Klinger et al., 2015; Patapoutian and Reichardt, 2001; Rohe et al.,
86 2013).
87
88 Here we used human induced pluripotent stem cell derived-neurons (hiPSC-Ns) to test the
89 hypothesis that *SORL1* plays a broader role in neuronal endosomal recycling. We use our
90 previously described *SORL1*-depleted hiPSC lines to generate hiPSC-Ns, which model the loss
91 of *SORL1* expression that occurs in AD(Knupp et al., 2020). Furthermore, we used previously
92 established cell lines engineered to overexpress *SORL1* 2-3-fold over wild-type levels(Young et
93 al., 2015) to test the effects of enhanced *SORL1* expression in hiPSC-Ns on these trafficking
94 pathways. Importantly, all cell lines are isogenic. We map the trafficking effects these
95 manipulations have on three specific receptors, APP, the GLUA1 subunit of the AMPA receptor,
96 and neurotrophin receptor TRKB, all of which are implicated in AD (Devi and Ohno, 2015; Dewar
97 et al., 1991; Ginsberg et al., 2019; Martin-Belmonte et al., 2020; Wakabayashi et al., 1999;
98 Yasuda et al., 1995).
99
100 Finally, we performed RNA-sequencing on the *SORL1* depleted cell lines to explore an unbiased
101 transcriptomics analysis induced by *SORL1* depletion. The results generally confirmed our

hypothesis, showing that *SORL1* is a broad regulator of endosomal recycling in neurons, a conclusion that has both pathogenic and therapeutic implications.

## METHODS

### Cell lines

***Cell lines generated by CRIPSR/Cas9 gene editing technology***

The generation of the cell lines used in this paper is described in our previously published work (Knupp et al., 2020) and consists of four clones: Two wild-type clones, designated clone A6 and clone A7, and two *SORL1*KO clones, designated clone E1 and clone E4. Cell lines were generated from our previously published and characterized CV background human induced pluripotent stem cell line(Young et al., 2015). This cell line is male and has a APOE ε3/ε4 genotype(Levy et al., 2007). All four clones were shown to have normal karyotypes and are routinely tested for mycoplasma (MycoAlert). The clones used in the experiments in this work are listed in the figure legends.

**CRISPR/Cas9 gRNA, ssODN, and Primer Sequences** gRNA: ATTGAACGACATGAACCCTC ssODN: GGGAATTGATCCCTATGACAAACCAAATACCATCTACATTGAACGACATGAACCCTCTGGC TACTCCACGTCTTCCGA AGTACAGATTTCTTCCAGTCCCGGGAAAACCAGGAAG Forward primer: ctctatcctgagtcaaggagtaac Reverse primer: ccttccaattcctgtgtatgc PCR amplifies 458 bp sequence. These sequences have been previously published in (Knupp et al., 2020)

***SORL1 overexpression cell lines*** Isogenic cell lines with overexpression of SORL1 were generated as previously described(Young et al., 2015). These lines are generated from the CV parental line, the same parental line as the *SORL1*KO cell lines were made from. Briefly, stable integration of SORL1 cDNA into the genome was achieved by using piggybac transposon system

128 (Systems Biosciences). Vector alone (WT) or vector with SORL1 cDNA (*SORL1*OE) constructs
129 were introduced into iPSCs by electroporation and stable cell lines were selected with puromycin
130 (2ug/ml) treatment. We obtained one SORL1OE stable cell line and one vector alone stable cell
131 line. For all overexpression experiments *SORL1*OE cells were compared to the vector alone
132 controls.
133
134 **hiPSC Neuronal Differentiation**
135 hiPSCs were differentiated to neurons using dual-SMAD inhibition(Chambers et al., 2009; Shi et
136 al., 2012). Briefly, hiPSCs were plated on Matrigel coated 6-well plates at a density of 3.5 million
137 cells per well and fed with Basal Neural Maintenance Media (1:1 DMEM/F12 + glutamine
138 media/neurobasal media, 0.5% N2 supplement, 1% B27 supplement, 0.5% GlutaMax, 0.5%
139 insulin-transferrin-selenium, 0.5% NEAA, 0.2% β-mercaptoethanol; Gibco, Waltham, MA) +
140 10mM SB-431542 + 0.5mM LDN-193189 (Biogems, Westlake Village, CA). Cells were fed daily
141 for seven days. On day eight, cells were incubated with Versene, gently dissociated using cell
142 scrapers, and passaged at a ratio of 1:3. On day nine, media was switched to Basal Neural
143 Maintenance Media and fed daily. On day 13, media was switched to Basal Neural Maintenance
144 Media with 20 ng/mL FGF (R&D Systems, Minneapolis, MN) and fed daily. On day sixteen, cells
145 were passaged again at a ratio of 1:3. Cells were fed until approximately day twenty-three. At this
146 time, cells were FACS sorted to obtain the CD184/CD24 positive, CD44/CD271 negative neural
147 precursor cell (NPC) population. Following sorting, NPCs were expanded for neural
148 differentiation. For cortical neuronal differentiation, NPCs were plated out in 10cm cell culture
149 dishes at a density of 6 million cells/10cm plate. After 24 hours, cells were switched to Neural
150 Differentiation media (DMEM-F12 + glutamine, 0.5% N2 supplement, 1% B27 supplement, 0.5%
151 GlutaMax) + 0.02ug/mL brain-derived neurotrophic factor (PeproTech, Rocky Hill, NJ) +
152 0.02ug/mL glial-cell-derived neurotrophic factor (PeproTech) + 0.5mM dbcAMP (Sigma Aldrich,
153 St Louis, MO). Media was refreshed twice a week for three weeks. After three weeks, neurons

154 were selected for CD184/CD44/CD271 negative population by MACS sorting and plated for
155 experiments. The data presented in this study represent 2-3 neuronal differentiations.
156
157 **Purification of Neurons**
158 Following three weeks of differentiation, neurons were dissociated with accutase and
159 resuspended in Magnet Activated Cell Sorting (MACS) buffer (PBS + 0.5% bovine serum albumin
160 [Sigma Aldrich, St Louis, MO] + 2mM ethylenediaminetetraacetic acid [Thermo Fisher Scientific,
161 Waltham, MA]). Following a modification of (Yuan et al., 2011), cells were incubated with PE-
162 conjugated mouse anti-Human CD44 and mouse anti-Human CD184 antibodies (BD
163 Biosciences, San Jose, CA) at a concentration of 5µl/10 million cells. Following antibody
164 incubation, cells were washed with MACS buffer and incubated with anti-PE magnetic beads (BD
165 Biosciences, San Jose, CA) at a concentration of 25µl/10 million cells. Bead-antibody complexes
166 were pulled down using a rare earth magnet, supernatants were selected, washed, and plated at
167 an appropriate density.
168
169 **DQ Red BSA assay for visualization of lysosomal degradation**
170 Lysosomal proteolytic degradation was evaluated using DQ Red BSA (#D-12051; Thermo Fisher
171 Scientific), a fluorogenic substrate for lysosomal proteases, that generates fluorescence only
172 when enzymatically cleaved in intracellular lysosomal compartments. hiPSC-derived neurons
173 were seeded at a density of 400,000 cells/well of a matrigel coated 48 well plate. After 24 hours,
174 cells were washed once with DPBS, treated with complete media containing either 10µg/ml DQ
175 Red BSA or vehicle (PBS) and incubated for 6 hours or 24 hours (Davis et al., 2021; Romano et
176 al., 2021; Tian et al., 2015)at 37°C in a 5% $CO_2$ incubator as described in(Marwaha and Sharma,
177 2017). At the end of 6 or 24 hours, cells were washed with PBS, fixed with 4% PFA and
178 immunocytochemistry was performed as described in methods. Cells were imaged using a Leica
179 SP8 confocal microscope and all image processing was completed with ImageJ software. Cell

180 bodies were identified by MAP2 labeling, and fluorescence intensity of DQ Red BSA was
181 measured in regions of the images containing the MAP2 label.
182
183 **Immunocytochemistry**
184 For immunocytochemistry, cells were fixed with 4% PFA for 20 minutes. Fixed cells were washed
185 three times with PBST (PBS with 0.05% tween 20), permeabilized with Triton X-100 in PBS for
186 15 minutes, washed twice again with PBST, blocked with 5% BSA in PBS at room temperature
187 for 1h and incubated with appropriate primary antibodies overnight at 4°C. The next day, cells
188 were incubated with appropriate secondary antibodies and 1µg/ml DAPI for 1 hour at RT, washed
189 three times with PBST and mounted on glass slides with Prolong Gold Antifade mountant
190 (#P36930; Thermo Fisher Scientific).
191
192 **Colocalization analysis**
193 To investigate colocalization with endo-lysosomal compartments, hiPSC-derived neurons were
194 labeled with markers specific for each intra-cellular compartment (EEA1 for early endosomes,
195 Rab7 for late endosomes, LAMP1 for lysosomes and Rab11 for recycling endosomes) using
196 immunocytochemistry. A minimum of 10 fields of confocal z-stack images were captured under
197 blinded conditions using a Yokogawa W1 spinning disk confocal microscope (Nikon) and a 100X
198 plan apochromat oil immersion objective. Median filtering was used to remove noise from images
199 and Otsu thresholding was applied to all images. Colocalization was quantified using the JACOP
200 plugin(Bolte and Cordelieres, 2006) in Image J software(Schindelin et al., 2012) and presented
201 as Mander's correlation coefficient.(Dunn et al., 2011; Manders et al., 1993). For all imaging
202 experiments the data was analyzed in a blinded manner.
203
204 **Cell Surface Staining:** Cell surface expression of GLUA1 and APP was determined using
205 immunocytochemistry and confocal microscopy. To label proteins at the cell surface, cells were

206 fixed with 4% PFA, washed and treated with primary and secondary antibodies as described in
207 the 'immunocytochemistry' section of methods. Permeabilization with 0.1% Triton X-100 was not
208 performed for this experiment. To label total protein levels, cells were fixed with 4% PFA, washed,
209 permeabilized with 0.1% Triton X-100 and treated with primary and secondary antibodies as
210 described in the 'immunocytochemistry' section of methods. Analysis of fluorescence intensity
211 was done using Image J software. Cell surface expression was represented as ratio of
212 fluorescence intensity measured under non-permeabilized conditions and fluorescence intensity
213 measured under permeabilized conditions. For all imaging experiments the data was analyzed in
214 a blinded manner.

215 **Multielectrode (MEA) assay**

216 hiPSC-derived neural progenitor cells were differentiated into neurons and neurons were purified
217 as previously described in methods. Purified neurons were mixed with unpurified neurons in a
218 ratio of 5:1 and this mixture was plated onto a matrigel coated 48 well MEA plate (Axion
219 Biosystems; # M768-tMEA-48W) at a cell density of 8000 cells/ul (total number of cells/well =
220 50,000). MEA-plated neurons were initially cultured in neural differentiation media. Media was
221 gradually switched to BrainPhys media (Stem cell technologies; # 05790) by replacing half of a
222 well's media twice a week. BrainPhys media was supplemented with B27, N2, BDNF, GDNF, and
223 db-cAMP.

224 **Multielectrode (MEA) analysis**

225 Electrical signals from neurons in the MEA plates were recorded twice a week using Axion
226 Biosystems Maestro Pro system. Signals were recorded at a sampling frequency of 12.5 kHz with
227 a 3 kHz Kaiser Window low pass filter and 200 Hz high pass filter. Spikes were detected using
228 Axion Axis Navigator recording software with the adaptive threshold method. Recordings were
229 analyzed using the Axion Neural Metric Tool. Firing rate data were limited to active electrodes
230 that detected a minimum of five spikes a minute. Firing rate data from all active electrodes in a
231 well were averaged for plotting and statistical testing.

232 **Antibodies**

233 The following primary antibodies were used: Early endosome antigen 1 (EEA1) at 1:500
234 (#610456; BD Biosciences); amyloid precursor protein (APP) at 1:500 (#ab32136; Abcam);
235 microtubule-associated protein 2 (MAP2) at 1:1000 (ab92434; Abcam); Ras-related protein Rab-
236 7a (Rab7) at 1:1000 (ab50533; Abcam); Ras-related protein Rab-11 (Rab11) at 1:250 (#610656;
237 BD Biosciences); Lysosome associated membrane protein-1 (LAMP1) at 1:250 (#sc 2011; Santa
238 Cruz); Tropomyosin receptor kinase B (TRKB; # ab18987; abcam) at 1:1000 ,GLUA1(#
239 MAB2263; Millipore sigma) at 1:500 andVPS35(Abcam; #ab97545) at 1:500. DAPI was used at
240 a final concentration of 0.1µg/ml (Alfa Aesar).

241

242 **Transferrin recycling assay**

243 To measure recycling pathway function, we utilized transferrin recycling assay as previously
244 described(Rapaport et al., 2010). Purified neurons were seeded at 400,000 cells/well of a 24 well
245 plate containing matrigel coated 12 mm glass coverslip/well. After 5 DIV, cells were washed once
246 with DMEM-F12 medium and incubated with starving medium (DMEM-F12 medium+25mM
247 HEPES+ 0.5% BSA) for 30 minutes at 37°C in a 5% $CO_2$ incubator to remove any residual
248 transferrin. Thereafter, cells were pulsed with either 100µg/ml transferrin from human serum
249 conjugated with Alexa Fluor™ 647(#T23366; Thermo Fisher Scientific) or vehicle (PBS) in
250 'starving medium'. At the end of 10 mins, cells were washed twice with ice-cold PBS to remove
251 any external transferrin and stop internalization of transferrin and washed once with acid stripping
252 buffer (25mM citric acid+24.5mM sodium citrate+280mM sucrose+0.01mM Deferoxamine) to
253 remove any membrane bound transferrin. Next, cells were either fixed in 4% PFA or 'Chase
254 medium' (DMEM-F12+50µM Deferoxamine+20mM HEPES+500µg/ml Holo-transferrin) was
255 added for different time points. Immunocytochemistry was done using MAP2 antibody to label
256 neurons, confocal images were captured using Leica SP8 confocal microscope under blinded
257 conditions. Fluorescence intensity of transferrin was measured using ImageJ software. Recycling

258 function was presented as transferrin fluorescence intensity as a percentage of the fluorescence
259 intensity measured at time zero.
260
261 **Measurement of lysosome and recycling endosome size**
262 Immunocytochemistry using antibodies for LAMP1 and MAP2 or RAB11 and MAP2 was
263 performed as described above. Using a Leica SP8 confocal microscope with an apochromatic
264 63X oil immersion lens, z-stack images were obtained under blinded conditions. For the LAMP1
265 analysis, 17-34 fields were analyzed for a total of **45 – 76** cells analyzed. For the RAB11 analysis,
266 15-30 fields were analyzed for a total of **59 – 124** cells analyzed. Vesicle size measurements were
267 performed using Cell Profiler software as previously described (Knupp et al., 2020) (McQuin et
268 al., 2018). Briefly, the vesicle channel was masked using the MAP2 channel and automated
269 segmentation algorithms were used to identify individual puncta. The pixel area of each puncta
270 was measured and is presented as mean area of all puncta per field.
271
272 **Statistical Analysis**
273 For all imaging experiments, data was collected and analyzed in a blinded manner. Data was
274 assessed for significance using parametric two-tailed unpaired Student's t-tests or two-way
275 ANOVA tests. Data is represented as mean $\pm$ standard deviation to show the spread of the data.
276 Significance was defined as a value of $p \leq 0.05$. All statistical analysis was completed using
277 GraphPad Prism software. Statistical details of individual experiments, including biological and
278 technical replicate information, can be found in the figure legends. All of the raw statistical data
279 for the experiments in this paper, including means, difference between the means $\pm$ SEM, and
280 95% confidence intervals are presented in Supplemental Table 1.
281
282 **RNA- sequencing analysis**
283 *RNA Extraction*

284 RNA was collected from 3 separate differentiations including a combination of two WT clones and
285 two *SORL1*KO clones. Each sample includes 2-3 technical replicates. RNA was collected from 2
286 million purified neurons for each sample. Purification of total RNA was completed using the
287 PureLink RNA Mini Kit (Thermo Fisher 12183018A). Assessment of purified RNA was completed
288 using a NanoDrop. Final RNA quantification was completed using the Quant-iT RNA assay
289 (Invitrogen) and RNA integrity analysis was completed using a fragment analyzer (Advanced
290 Analytical).
291
292 *Library Prep and Sequencing*
293 Library preparation was completed using the TruSeq Stranded mRNA kit (Illumina RS-122-2103)
294 per manufacturer instructions. Sequencing was performed on a NovaSeq 6000 instrument.
295
296 *Data analysis*
297 Raw reads were aligned to GRCh38 with reference transcriptome GENCODE release 29 using
298 STAR v2.6.1d(Dobin et al., 2013). Gene-level expression quantification is generated by RSEM
299 v1.3.1(Li and Dewey, 2011). Genes with fewer than 20 normalized reads across all samples were
300 omitted from further analysis. We did observe variation in the transcriptome based on
301 differentiation (Supplemental Figure 3A), however this was corrected for using the sva
302 package(Leek et al., 2012).
303
304 To identify differentially expressed genes (DEGs), we used DESeq(Anders and Huber, 2010).
305 Briefly, we fit two models: a null model where gene expression only depends on batch effects
306 (i.e., differentiation), and an alternative model where gene expression depends on both genotype
307 (*SORL1*KO vs. WT) and batch effects. Chi-squared tests were performed to compare both fits,
308 and we declare a gene as differentially expressed only when the alternative model fits the
309 expression data better. DEGs are defined as genes with false discovery rate less than 0.05 and

310 fold change greater than 1.5. The top gene ontology package(Alexa et al., 2006) and the SynGO
311 synaptic gene ontology annotations(Koopmans et al., 2019) were used to identify GO terms that
312 were enriched. GO terms were tested according to the Fisher's exact test. Finally, we mapped
313 DEGs onto receptor-ligand interaction diagrams generated by Ramilowski et al(Ramilowski et al.,
314 2015) using the igraph plugin(Csardi G, 2006). To compare the amount of down-regulated vs. up-
315 regulated genes we used a 2-sample test for equality of proportions with continuity correction in
316 R.
317

318 **RESULTS**

319 ***SORL1* depletion increases neuronal cargo localization in early endosomes.**

320 Using CRISPR/Cas9 genome editing techniques, we previously generated hiPSC-derived
321 neurons (hiPSC-Ns) deficient in *SORL1* expression due to indels introduced in exon 6. We
322 demonstrated that loss of *SORL1* expression in these neurons leads to enlarged early endosomes
323 and an increased colocalization of APP within early endosomes, indicative of endosomal traffic
324 jams(Knupp et al., 2020). We utilized these same cell lines (hereafter referred to as *SORL1*KO
325 and their guide-matched isogenic wild-type clones referred to as WT) to examine localization of
326 the BDNF receptor TRKB and the GLUA1 subunit of the neuronal AMPA receptor. TRKB has
327 been shown to bind to SORLA and this interaction mediates trafficking of TRKB to synaptic
328 plasma membranes(Rohe et al., 2013). GLUA1 is trafficked via the retromer complex, of which
329 SORLA is an adaptor protein(Fjorback et al., 2012; Temkin et al., 2017) and both of these cargo
330 are important in maintaining healthy neuronal function. Because we previously observed an
331 increase in APP localization in early endosomes, resulting in a decrease in localization in
332 downstream vesicles such as Ras-related protein (Rab)7+ late endosomes with *SORL1*
333 depletion(Knupp et al., 2020), we performed an immunocytochemical analysis of both TRKB and
334 GLUA1 localization with the early endosome marker EEA1. Similar to our previous observations
335 for APP, we documented significantly increased localization of both TRKB (Figure 1A) and GLUA1

336 (Figure 1B) in early endosomes in *SORL1*KOneurons as compared to isogenic WT control
337 neurons. Accumulation of neuronal cargo in early endosomes is indicative of endosomal traffic
338 jams, which are thought to impact the transit of cellular cargo through other arms of the endo-
339 lysosomal network. Due to SORLA's role as an adaptor protein for the retromer complex, we also
340 examined whether *SORL1* depletion led to changes in retromer subunit localization. We observed
341 that VPS35, a core subunit of the retromer cargo recognition complex is also mis-localized to
342 early endosomes, similar to what we observed for APP, TRKB, and GLUR1 (Supplemental Figure
343 1).
344
345 **Modulating *SORL1* expression impacts cargo trafficking throughout the endo-lysosomal**
346 **system**
347 The early endosome serves as a hub in which internalized cargo can be retrogradely transported
348 to the trans-Golgi, recycled back to the cell surface or degraded as endosomes mature into late
349 endosomes and lysosomes(Mayle et al., 2012). We have previously observed that APP
350 localization within the trans-Golgi network was decreased in *SORL1*KO neurons(Knupp et al.,
351 2020). Here we tested whether trafficking to the degradative arm of the endo-lysosomal network
352 was affected in our *SORL1*KO neurons. Trafficking of substrates out of the early endosome to
353 late endosomes and, subsequently, lysosomes is important for protein degradation and SORLA
354 has been previously implicated in promoting Aβ degradation via lysosomes(Caglayan et al.,
355 2014). We treated *SORL1* deficient neurons with DQ Red BSA, a proteolysis sensitive fluorogenic
356 substrate that generates fluorescence only when enzymatically cleaved in intracellular lysosomal
357 compartments. Since substrate degradation primarily occurs in lysosomes, altered fluorescence
358 intensity of this reagent is a readout of altered lysosomal degradation(Marwaha and Sharma,
359 2017). We treated neurons with DQ Red BSA for 6 and 24 hours and analyzed fluorescence
360 intensity using confocal microscopy. Consistent with loss of *SORL1* leading to endosomal traffic
361 jams, we observed a significant reduction of DQ Red BSA fluorescence intensity at both time

362 points in *SORL1*KO neurons compared to isogenic WT controls (Figure 2A). We next performed
363 immunocytochemical staining to quantify the colocalization of our selected neuronal cargo with
364 Rab7, a marker of late endosomes, and LAMP1 (Lysosomal Associated Membrane Protein 1), a
365 lysosome marker. We show a significant decrease in co-localization of TRKB (Figure 2B) and
366 GLUA1 (Figure 2C) with Rab7. This result is consistent with our previous observation for APP
367 (Knupp et al., 2020). We analyzed colocalization of these cargo with LAMP1 and we observed a
368 significant decrease with APP (Figure 2D) and TRKB (Figure 2E) and a trend of a decrease with
369 GLUA1 (Figure 2F). These data indicate some fluidity in the network but suggest that trafficking
370 of APP, TRKB and GLUA1 to late endosomes/lysosomes is all decreased by *SORL1*KO, although
371 GLUA1 may be more likely to be trafficked to cell surface pathways or utilizes other adaptor
372 proteins for late endosome to lysosomal trafficking. These changes in localization are not due to
373 changes in expression of cargo. We have previously shown that APP levels do not change in
374 *SORL1*KO neurons(Knupp et al., 2020) and also show here that protein expression of TRKB and
375 GLUA1 are not different (Supplemental Figure 3).
376
377 We next utilized previously generated cell lines that overexpress *SORL1* cDNA using the
378 piggybac transposon system(Young et al., 2015) to test whether increased *SORL1* expression
379 may enhance the trafficking pathways that are impaired in the *SORL1*KO neurons. Importantly,
380 the *SORL1* overexpressing (*SORL1*OE) cell line and control were generated in the same genetic
381 background as our *SORL1*KO and isogenic WT cell lines. Interestingly, while there was no effect
382 of *SORL1* overexpression on DQ Red BSA fluorescence at the earlier time point (6 hours), we
383 did see a significant enhancement of DQ RED BSA trafficking at the 24-hour time point (Figure
384 3A). In accordance, we observed significantly increased localization of our studied cargo with late
385 endosomal and lysosomal markers in the *SORL1*OE neurons (Figure 3 B-G).
386 Lysosome size can influence lysosome function and is altered in AD(de Araujo et al., 2020; Hwang
387 et al., 2019). Similarly, location and number of lysosomes within neurons can alter degradative

activity (Cheng et al., 2018; Farfel-Becker et al., 2019; Gowrishankar et al., 2015; Yap et al., 2018) and in some cases, altered lysosomal distribution may represent an early neuropathological defect(Zigdon et al., 2017).Recently, loss of *SORL1* in hiPSC neurons was shown to contribute to lysosome dysfunction as indicated by both increased lysosome size and number as well as decreased cathepsin-D activity(Hung et al., 2021). Therefore, we first analyzed LAMP1-immunopositive puncta and also documented a significant increase in lysosome size and number in our *SORL1*KO neurons (Supplemental Figure 2A). Interestingly, although the number of lysosomes marked by LAMP1 puncta is increased in *SORL1KO* neurons, we did not observe a significant change in LAMP1 protein expression (Supplemental Figure 3). This may be partially explained by differences in autophagy in SORL1 KO neurons which we did not examine in this study but that has been previously reported(Hung et al., 2021) and further underscores the dynamic complexity of the endo-lysosomal network.

Next, we analyzed co-localization of Cathepsin-D and LAMP1 to determine if loss of *SORL1* expression leads to altered Cathepsin-D trafficking in neurons. Retromer trafficking is required to deliver one of the most abundant lysosomal proteases, pro-cathepsin D, to lysosomes via the mannose-6-phosphate receptor (M6PR)(Qureshi et al., 2018; Seaman, 2004). The SORLA protein has GGA domains similar to that of M6PR(Spoelgen et al., 2006), and mis-trafficking of Cathepsin-D to lysosomes could affect the maturation and degradative capacity of these organelles. Therefore, we analyzed co-localization of Cathepsin-D and LAMP1 to determine if loss of *SORL1* expression leads to altered Cathepsin-D trafficking in neurons. However, we did not observe a change in Cathepsin-D colocalization between WT and *SORL*1KO (Supplemental Figure 2B).

Taken together, our data suggest that *SORL1* loss in neurons reduces trafficking of cargo out of the early endosome to the late endosome and lysosome, contributing to lysosome stress as

414 evidenced by an increase in size and number in these conditions while the decreased cathepsin-
415 D activity observed upon *SORL1* loss(Hung et al., 2021) may not be due to impairment of
416 lysosomal trafficking of the enzyme.
417
418 **Loss of *SORL1* impacts the endosomal recycling pathway**
419 Another route out of the early endosome is via the endocytic recycling complex (ERC) which can
420 send cargo either to the cell surface or to the trans-Golgi network(Grant and Donaldson, 2009;
421 Mallard et al., 1998; Marsh et al., 1995; Maxfield and McGraw, 2004). To directly examine if
422 *SORL1* expression alters recycling function, we performed a transferrin recycling assay using
423 confocal microscopy. Transferrin can be recycled via a fast pathway within approximately 5-10
424 minutes after being internalized or via a slower pathway involving the ERC over longer periods of
425 time(Ouellette and Carabeo, 2010; Sonnichsen et al., 2000). We examined the fluorescence
426 intensity of Alexa Fluor 647-conjugated transferrin over a 40-minute time course in WT and
427 *SORL1*KO neurons and observed that a higher percentage of intracellular fluorescent transferrin
428 persisted in *SORL1*KO neurons at both early and later time points as compared to WT neurons,
429 indicating reduced recycling pathway function (Figure 4A). Cargo destined for the cell surface can
430 transit the ERC via Rab11+ recycling endosomes (Ren et al., 1998). Altered size of recycling
431 endosomes can be indicative of dysfunctional recycling of cargo through these compartments.
432 We tested whether loss of *SORL1* expression affected the size of Rab11+ recycling endosomes.
433 Interestingly, we observed a significant increase in the size of Rab11+ recycling endosomes,
434 although there was no change in Rab11 protein expression in the *SORL1*KO neurons (Figure 4B,
435 Supplemental Figure 3), suggesting that this endosomal compartment is also under stress. To
436 test if increased size is due to abnormal cargo trafficking through recycling endosomes, we
437 assessed colocalization of APP, TRKB and GLUA1 with Rab11 and observed increased co-
438 localization of all three cargo with Rab11+ structures in *SORL1*KO neurons compared to WT
439 neurons (Figure 4C-E). Together, these data demonstrate that loss of *SORL1* impacts neuronal

440 recycling endosome pathways by causing traffic jams in the recycling endosomes, similar to the
441 effect that *SORL1* loss has on early endosomes.
442
443 ***SORL1* depletion reduces cell surface levels of cargo.**
444 Together, our data indicate that *SORL1*KO neurons have impaired cargo recycling with increased
445 retention of cargo in recycling endosomes. These observations led us to test whether this cargo
446 was indeed trafficked to the cell surface. A portion of APP has been shown to return to the cell
447 surface via recycling endosomes(Das et al., 2016) and SORLA can interact with the sorting nexin
448 SNX27 to return APP to the cell surface(Das et al., 2016; Huang et al., 2016), although in that
449 study the exact compartment was not described. Furthermore, recycling endosomes are the
450 source for AMPA receptors during long-term potentiation(Park et al., 2004). We therefore
451 examined cell surface levels of APP and GLUA1 using immunofluorescence and confocal
452 microscopy. We documented a significant decrease in cell surface staining of both APP (Figure
453 5A) and GLUA1 (Figure 5B) in *SORL1*KO neurons as compared to WT, consistent with our
454 hypothesis that SORLA is involved in regulating traffic from recycling endosomes. Due to the
455 importance of GLUA1 in the formation of functional excitatory synapses, we next analyzed
456 neuronal activity by culturing *SORL1*KO and isogenic WT neurons on multi-electrode array (MEA)
457 plates. Interestingly, we observed an early increase in the mean firing rate of *SORL1*KO neurons
458 at an early time point (27 days post-plating) however neuronal firing in *SORL1*KO neurons was
459 significantly reduced at a later time point (66 days post-plating) (Figure 5C) suggesting that
460 synaptic activity may be partially impaired in these cells.
461
462 ***SORL1* overexpression enhances endosomal recycling**
463 Defects in cell surface recycling have severe consequences in neurons, especially as these
464 processes are necessary for healthy neuronal function and enhancing pathways that promote
465 endosomal recycling in neurons may be beneficial. Using our *SORL1*OE neurons we analyzed

466 recycling function using the transferrin recycling assay and observed that *SORL1*OE neurons
467 showed significantly faster transferrin recycling (Figure 6A). We next tested whether colocalization
468 of cargo with recycling endosomes and cell surface recycling was altered between *SORL1*OE
469 and WT neurons. Interestingly, the size of Rab11+ recycling endosomes was significantly smaller
470 in *SORL1*OE neurons (Figure 6B) possibly indicating that increased *SORL1* expression is clearing
471 cargo more rapidly from this compartment. We observed a significant increase in localization of
472 cargo with Rab11+ recycling endosomes (Figure 6C-E). While this result was initially surprising,
473 as we also saw increased colocalization with Rab11+recycling endosomes in our *SORL1*KO
474 neurons (Figure 4C-E), we further documented a significant increase of APP and GLUA1 on the
475 cell surface compared to WT neurons with only endogenous *SORL1* expression (Figure 6F and
476 6G), as opposed to decreased APP and GLUA1 localization on the cell surface in *SORL1*KO
477 neurons (Figure 5A and 5B). These results suggest that cell surface trafficking via a Rab11
478 pathway is enhanced by increased *SORL1* expression and that a crucial action of SORLA is the
479 trafficking out of recycling endosomes. Thus, our data support a critical role for SORLA for
480 trafficking cargo from recycling endosomes to the cell surface. In addition, we show for the first
481 time that SORLA levels may regulate cell surface recycling of AMPA receptor subunits in human
482 neurons.
483
484 ***SORL1* depletion affects gene expression**.
485 To determine a more global effect of chronic *SORL1* loss in human neurons, we performed bulk
486 RNA sequencing of *SORL1*KO neurons compared to WT neurons. Interestingly, we observed that
487 there were significantly more down-regulated genes in *SORL1*KO neurons than upregulated ones
488 (Supplemental Figure 4B). While none of the cargo we explicitly studied in this work was
489 differentially expressed, GO analysis showed that the top downregulated molecular function
490 pathways in the *SORL1*KO cells were related to receptor-ligand activity and extracellular matrix
491 organization (Figure 7A). The top upregulated molecular function pathways were related to ion

492 channel activity (Figure 7B). To understand these data in the context of an integrated network,
493 we used an analysis method that infers ligand receptor interactions from bulk RNA-seq
494 data(Ramilowski et al., 2015; Wang et al., 2020). We observed several nodes of altered receptor-
495 ligand interactions that indicate altered cell surface recycling and neurotrophic activity (Figure
496 7C). These include alterations in β-integrin signaling, which is consistent with previous work
497 showing reduced β-integrin on the cell surface in *SORL1*KO cancer cells(Pietila et al., 2019), and
498 altered interactions in ephrins/ephrin receptors, also corroborating previous work implicating
499 *SORL1* expression in ephrin signaling and synapse regulation(Huang et al., 2017). Our analysis
500 also showed nodes with alterations in nerve growth factor/nerve growth factor receptor
501 (NGF/NGFR) and fibroblast growth factor/fibroblast growth factor receptor (FGF/FGFR) signaling,
502 indicating alterations in neurotrophin and growth factor signaling and suggesting that the presence
503 of endosomal traffic jams in *SORL1*KO neurons may ultimately impact multiple pathways
504 important for neuronal health and development. Because we documented a decrease of GLUA1
505 puncta on the cell surface and observed altered neuronal activity on MEAs, we further mined our
506 RNA-seq data for genes involved in synaptic function. Interestingly when we performed
507 enrichment analysis, we observed that pathways associated with synaptic function were
508 upregulated in *SORL1*KO neurons (Supplemental Figure 5).
509

510 **DISCUSSION**

511 Trafficking through the endo-lysosomal network regulates intra-cellular location of proteins,
512 dictating their homeostasis, function and influence on cellular physiology. Functional studies by
513 our group and others document endosomal abnormalities in hiPSC-derived neuronal models of
514 AD(Hung et al., 2021; Knupp et al., 2020; Kwart et al., 2019). Emerging from this evidence is the
515 role of *SORL1* as an endosomal gene that plays essential roles in mediating cargo trafficking.
516 Recent work has implicated *SORL1* as AD's fourth causal gene(Olav M. Andersen, 2021;

517 Scheltens et al., 2021), and of these genes it is the only one linked to the common late-onset form
518 of the disease. Understanding *SORL1*'s function is paramount for understanding AD's pathogenic
519 mechanisms and for potential therapeutic interventions.
520
521 Acting as an adaptor molecule of the retromer trafficking complex, SORLA has already been
522 pathogenically linked to AD by its role in recycling APP out of endosomes(Andersen et al., 2005;
523 Herskowitz et al., 2012; Offe et al., 2006). This current work and our previous study(Knupp et al.,
524 2020) shows that *SORL1* depletion leads to increased APP localization in early and recycling
525 endosomes. By lengthening the residence time of APP in these endosomal compartments,
526 accelerated amyloidogenic cleavage of APP occurs due to the close proximity of APP and
527 BACE1(Sun and Roy, 2018). Indeed, loss of *SORL1* leads to the accumulation of Aβ peptides,
528 an antecedent of 'amyloid pathology' (Andersen et al., 2005; Knupp et al., 2020; Rogaeva et al.,
529 2007b). We hypothesized that loss of *SORL1* in neurons would impact other cargo important for
530 healthy neuronal function. To test this hypothesis, in addition to APP, we examined localization
531 of the neurotrophin receptor TRKB and the GLUA1 subunit of the AMPA receptor and also
532 observed that these proteins are increased in early endosomes (Figure. 1). These cargo link to
533 another key pathology of AD: neurodegeneration, a slowly progressive process that begins with
534 synaptic dysfunction characterized by glutamate receptor loss, which then progresses to synaptic
535 loss before ultimately, over years, leading to widespread neuronal cell death (Selkoe, 2002).
536
537 The early endosome is considered the central station in the sorting and trafficking of cargo
538 throughout the many stations of the endo-lysosomal system. While the early endosome is the
539 station that is affected first and foremost in AD, it is not surprising that a primary dysfunction in
540 this central station will secondarily influence trafficking throughout the system including the
541 recycling and degradative pathways. Indeed, SORLA was shown to traffic Aβ to lysosomes in

542 neuroblastoma cells, a function that is impaired by an AD-associated variant(Caglayan et al.,
543 2014). Our work presented in this study, along with other recent work(Hung et al., 2021) also
544 supports a role for *SORL1* in lysosomal trafficking in neurons. We observe a decrease in the pH-
545 sensitive fluorogenic substrate DQ RED BSA in our *SORL1*KO neurons and decreased
546 localization of APP, TRKB, and GLUA1 in late endosomes and lysosomes in *SORL1*KO neurons
547 and that this is reversed in *SORL1*OE neurons (Figure. 2, Figure. 3). We interpret our functional
548 and colocalization data to suggest that loss of *SORL1* expression mainly affects trafficking of
549 cargo to lysosomes, but our data does not rule out a role of SORLA in neuronal lysosome function.
550 Hung et al., reported decreased Cathepsin-D activity in *SORL1* deficient neurons, suggesting that
551 *SORL1* loss directly impacts lysosome function(Hung et al., 2021). While we did not observe a
552 difference in Cathepsin-D localization to lysosomes, it is important to note that that LAMP1 only
553 partially colocalizes with Cathepsin-D in neurons (Cheng et al., 2018). Furthermore, the loss of
554 proteolytic activity evidenced by decreased intensity of DQ Red BSA in *SORL1*KO neurons may
555 not be completely due to reduced trafficking to lysosomes but could be a result of abnormal
556 lysosomal function as DQ Red BSA is internalized by a process called macropinocytosis wherein
557 macropinosomes can be directly trafficked to lysosomes (Hamasaki et al., 2004; Lorenzen et al.,
558 2010; Racoosin and Swanson, 1993). Interestingly, while we did not observe an effect on DQ Red
559 BSA at a shorter time point in *SORL1*OE neurons, we did see increased fluorescence of this
560 reagent at a 24-hour time-point (Figure. 3), suggesting that overtime, increased SORL1
561 expression impacts lysosome trafficking and/or function in cortical neurons.
562
563 Our experiments also point to *SORL1*'s role in cell surface recycling. By using a prototypical cargo,
564 transferrin, we demonstrate a reciprocal role between loss and enhancement of *SORL1*
565 expression in cell surface recycling. Specifically, we show that *SORL1*KO neurons have defects
566 in transferrin recycling at both early (10-minute) and late (40-minute) time points while *SORL1*OE
567 neurons have faster recycling at these time points (Figure 4, Figure 6). This suggests that SORLA

568 functions in both fast and slow endosomal recycling. Our data further implicates the recycling
569 pathway by showing that modulation of SORLA expression affects recycling endosome size and
570 the amount of cargo (APP, TRKB and GLUA1) localized to recycling endosomes (Figure. 4,
571 Figure. 6).
572
573 Endocytic recycling comprises returning cargo, primarily membrane proteins, to the cell
574 surface(Cullen and Steinberg, 2018). We studied a canonical SORLA cargo, APP, and show that
575 loss of *SORL1* expression results in reduced cell surface APP while enhanced expression
576 increases cell surface APP (Figure 5). These results corroborate previous work showing that
577 *SORL1* and SNX27 work to return APP to the cell surface(Das et al., 2016; Huang et al., 2016)
578 in a human model.
579
580 We also show that *SORL1* plays a role in recycling glutamate receptors (Figure. 5) This finding is
581 critically important as recent work indicates that in mouse cortical neurons, SORLA interacts with
582 a neuronal specific retromer subunit, VPS26b, to promote recycling of glutamate
583 receptors(Simoes S., 2021). In our cortical neurons when *SORL1* is depleted, there is a reduction
584 of GLUA1 subunits on the cell surface and this may result in synaptic impairment. MEA data
585 comparing *SORL1*KO and isogenic WT neurons shows alterations in weighted mean firing rate
586 as neurons mature (Figure 5). Interestingly, we observed an increase in neuronal firing at an early
587 time point and a significant decrease in firing at a later time point. *SORL1*KO mice live to
588 adulthood but have been described to have some deficits in learning and memory that may also
589 be age dependent(Glerup et al., 2013; Hojland et al., 2018). Some of these alterations could be
590 explained by compensatory expression changes ion channels or synaptic genes induced by
591 chronic loss of *SORL1* during the course of neuronal differentiation from pluripotent stem cells.
592 Our RNA-seq data does show up-regulation of ion channels and channel activity (Figure. 7).
593 Interestingly, when we further interrogated our RNA-seq data for pathways enriched in synaptic

594 function using the SynGo database (Koopmans 2019), we observed an upregulation of
595 differentially expressed genes in synaptic pathways (Supplemental Fig. 5). This data suggests
596 that *SORL1*KO neurons may attempt to compensate for altered trafficking of synaptic receptors
597 by upregulating gene expression.

598 Our unbiased transcriptomic screen further supported that neurotrophic signaling and cell
599 surface recycling pathways are impacted by *SORL1* deficiency (Figure 7). The SORLA
600 cytoplasmic tail has been shown to translocate to the nucleus and activate transcription in a
601 reporter gene assay(Bohm et al., 2006). Despite this, distinct genes regulated by SORLA are
602 not known. Rather than looking for a direct effect on gene regulation, our goal for the analysis
603 was to determine the global effect of *SORL1* loss or overexpression on neuronal networks.
604 Indeed, our data does not show that the specific cargo proteins described here are differentially
605 expressed. However, the analysis does indicate that loss of *SORL1* in human neurons impacts
606 cell surface networks, including receptor ligand interactions in neurotrophic and growth factor
607 pathways, β-integrin signaling, and ephrin signaling. This corroborates previous work and the
608 altered networks we observe impact neuronal health, axonal guidance, and synapse
609 formation(Huang et al., 2017; Huang et al., 2006; Pietila et al., 2019).

610 Importantly, enhancing SORL1 expression improves cell surface trafficking of GLUA1 (Figure 6).
611 Trafficking of glutamate receptors is an event that is critical for preventing synaptic dysfunction
612 and synaptic loss, thus our results link *SORL1* to AD's early-stage neurodegenerative process.
613 Since retromer-dependent glutamate receptor recycling has been shown to occur independent of
614 APP(Temkin et al., 2017), our previous and current results suggest that *SORL1* mutations can,
615 at least in principle, drive two key AD pathologies, amyloid pathology and synaptic pathology,
616 through parallel mechanisms(Small and Petsko, 2020).

617 We summarize our findings in Figure. 8. However, our study has certain limitations. For example,
618 our results encompass only one human genome. Future studies will benefit from looking at
619 *SORL1* deficiency or overexpression in multiple human genetic backgrounds. Furthermore, in this
620 work we are describing purely neuronal phenotypes although *SORL1* is expressed in other CNS
621 cells. Future work looking at cell- autonomous and non-cell autonomous mechanisms of *SORL1*
622 depletion or overexpression in human glial or brain organoid models will be informative.

623 **CONCLUSIONS**

624 In this work, we report that *SORL1* depletion affects endosomal trafficking by retaining cargo in
625 early and recycling endosomes and impacts cell surface recycling and lysosomal trafficking of
626 neuronal cargo. In particular, we demonstrate that *SORL1* expression in neurons affects cell
627 surface localization of GLUA1, a phenotype that may ultimately impact synaptic dysfunction and
628 neurodegeneration in AD. Interestingly, increasing *SORL1* expression enhances endosomal
629 recycling and increases cell surface GLUA1. While the secondary downstream effects induced
630 by *SORL1* depletion in the endo-lysosomal system are interesting and likely relevant to AD's
631 ultimate pathogenesis, from a therapeutic perspective it is best to target *SORL1*'s primary defect,
632 which seems to localize to the endosomal recycling pathway. Interestingly, recent biomarker
633 studies suggest that defects in retromer-dependent endosomal recycling occur in a majority of
634 patients with 'sporadic' AD(Simoes et al., 2020), suggesting that the observed *SORL1*-induced
635 defects may generalize across early and late onset forms of the disorder. Collectively, our results
636 support the conclusion that *SORL1*, and the retromer-dependent pathway in which it functions, is
637 a valid therapeutic target and interventions directed at this pathway may ameliorate endosomal
638 recycling defects that seem to act as, at least, one primary driver of AD.

639 **ABBREVIATIONS**

640 AD: Alzheimer's Disease; SORL1: Sortilin-related receptor 1; SORLA: Sortilin-related receptor
641 with A-type repeats; APP: Amyloid Precursor Protein; TRKB: Tropomyosin Related Kinase B;
642 GLUA1: Glutamate receptor subunit AMPA1; AMPA: α-amino-3-hydroxy-5-methyl-4-

643 isoxazolepropionic acid; OE: Overexpression; KO: Knock-out; WT: Wild-type; LAMP1:
644 Lysosome-associated membrane glycoprotein 1; M6PR: mannose-6-phosphate receptor; GGA:
645 Golgi-Localized γ-Ear-Containing ARF-Binding; Rab: Ras-related protein.

646 **DECLARATIONS**

647 **Ethics Approval and Consent to Participate**

648 Not applicable

649 **Consent for Publication**

650 Not applicable

651 **Availability of Data and Material**

652 All raw and processed RNA-seq data has been deposited at the NCBI Gene Expression Omnibus
653 (GSE180793). The data sets used and/or analyzed during the current study are available from
654 the corresponding author on reasonable request.

655 **Availability of Supporting Material**

656 All supporting data and material in the current study are available from the corresponding author
657 on reasonable request.

658 **Competing Interests**

659 The authors declare no competing interests

660 **Acknowledgements**

661 We thank Dr. Harald Frankowski, Dr. Yoshito Kinoshita, Ms. Shannon Rose, Ms. Eden
662 Cruickshank and all members of the Young Laboratory for critical discussions and feedback
663 during the preparation of this manuscript. We also thank Dr. Scott A. Small and Dr. Gregory A.
664 Petsko for critical comments, discussions and feedback on this work. We would like to
665 acknowledge the UW SLU Cell Analysis Facility and the Garvey Imaging Core at the UW Institute
666 for Stem Cell and Regenerative Medicine. This work was supported by a NIH grant
667 (R01AG062148) and a BrightFocus Foundation grant (A2018656S) to J.E.Y., a Biogen

668 Sponsored Research Agreement to J.E.Y., a Retromer Therapeutic Sponsored Research
669 Agreement to J.E.Y. and NIH traning grant (T32AG052354) to A.K. and a generous gift from the
670 Ellison Foundation (to UW).

671 **Author Contributions:**

672 Conceptualization: J.E.Y., S.M, A.K. Microscopy analysis: S.M, A.K., and D.W.H. RNA-seq
673 analysis and bioinformatics: Y.W and A.K. Methodology: S.M., A.K., M.S., C.A.W., C.K. Writing-
674 Original Draft: S.M., A.K. and J.E.Y. Writing-Reviewing and editing: J.E.Y., S.M., A.K. Funding
675 Acquisition: J.E.Y. and A.K. Supervision: J.E.Y. All authors read and approved the final
676 manuscript.

677

678 **REFERENCES**

679 Alexa, A., Rahnenfuhrer, J., and Lengauer, T. (2006). Improved scoring of functional groups from
680 gene expression data by decorrelating GO graph structure. Bioinformatics *22*, 1600-1607.
681 Anders, S., and Huber, W. (2010). Differential expression analysis for sequence count data.
682 Genome Biol *11*, R106.
683 Andersen, O.M., Reiche, J., Schmidt, V., Gotthardt, M., Spoelgen, R., Behlke, J., von Arnim, C.A.,
684 Breiderhoff, T., Jansen, P., Wu, X.*, et al.* (2005). Neuronal sorting protein-related receptor
685 sorLA/LR11 regulates processing of the amyloid precursor protein. Proc Natl Acad Sci U S A *102*,
686 13461-13466.
687 Bohm, C., Seibel, N.M., Henkel, B., Steiner, H., Haass, C., and Hampe, W. (2006). SorLA signaling
688 by regulated intramembrane proteolysis. J Biol Chem *281*, 14547-14553.
689 Bolte, S., and Cordelieres, F.P. (2006). A guided tour into subcellular colocalization analysis in light
690 microscopy. J Microsc *224*, 213-232.
691 Caglayan, S., Takagi-Niidome, S., Liao, F., Carlo, A.S., Schmidt, V., Burgert, T., Kitago, Y.,
692 Fuchtbauer, E.M., Fuchtbauer, A., Holtzman, D.M.*, et al.* (2014). Lysosomal sorting of amyloid-
693 beta by the SORLA receptor is impaired by a familial Alzheimer's disease mutation. Science
694 translational medicine *6*, 223ra220.
695 Cataldo, A.M., Peterhoff, C.M., Troncoso, J.C., Gomez-Isla, T., Hyman, B.T., and Nixon, R.A. (2000).
696 Endocytic pathway abnormalities precede amyloid beta deposition in sporadic Alzheimer's
697 disease and Down syndrome: differential effects of APOE genotype and presenilin mutations. Am
698 J Pathol *157*, 277-286.
699 Chambers, S.M., Fasano, C.A., Papapetrou, E.P., Tomishima, M., Sadelain, M., and Studer, L.
700 (2009). Highly efficient neural conversion of human ES and iPS cells by dual inhibition of SMAD
701 signaling. Nat Biotechnol *27*, 275-280.

Cheng, X.-T., Xie, Y.-X., Zhou, B., Huang, N., Farfel-Becker, T., and Sheng, Z.-H. (2018). Characterization of LAMP1-labeled nondegradative lysosomal and endocytic compartments in neurons. J Cell Biol *217*, 3127-3139.

Choi, J.H., Kaur, G., Mazzella, M.J., Morales-Corraliza, J., Levy, E., and Mathews, P.M. (2013). Early endosomal abnormalities and cholinergic neuron degeneration in amyloid-beta protein precursor transgenic mice. J Alzheimers Dis *34*, 691-700.

Csardi G, N.T. (2006). The igraph software package for complex network research. InterJournal, Complex systems *1695*.

Cullen, P.J., and Steinberg, F. (2018). To degrade or not to degrade: mechanisms and significance of endocytic recycling. Nat Rev Mol Cell Biol *19*, 679-696.

Das, U., Wang, L., Ganguly, A., Saikia, J.M., Wagner, S.L., Koo, E.H., and Roy, S. (2016). Visualizing APP and BACE-1 approximation in neurons yields insight into the amyloidogenic pathway. Nat Neurosci *19*, 55-64.

Davis, S.E., Roth, J.R., Aljabi, Q., Hakim, A.R., Savell, K.E., Day, J.J., and Arrant, A.E. (2021). Delivering progranulin to neuronal lysosomes protects against excitotoxicity. Journal of Biological Chemistry *297*.

de Araujo, M.E.G., Liebscher, G., Hess, M.W., and Huber, L.A. (2020). Lysosomal size matters. Traffic *21*, 60-75.

Devi, L., and Ohno, M. (2015). TrkB reduction exacerbates Alzheimer's disease-like signaling aberrations and memory deficits without affecting β-amyloidosis in 5XFAD mice. Translational psychiatry *5*, e562-e562.

Dewar, D., Chalmers, D.T., Graham, D.I., and McCulloch, J. (1991). Glutamate metabotropic and AMPA binding sites are reduced in Alzheimer's disease: an autoradiographic study of the hippocampus. Brain Res *553*, 58-64.

Dobin, A., Davis, C.A., Schlesinger, F., Drenkow, J., Zaleski, C., Jha, S., Batut, P., Chaisson, M., and Gingeras, T.R. (2013). STAR: ultrafast universal RNA-seq aligner. Bioinformatics *29*, 15-21.

Dodson, S.E., Gearing, M., Lippa, C.F., Montine, T.J., Levey, A.I., and Lah, J.J. (2006). LR11/SorLA expression is reduced in sporadic Alzheimer disease but not in familial Alzheimer disease. J Neuropathol Exp Neurol *65*, 866-872.

Dunn, K.W., Kamocka, M.M., and McDonald, J.H. (2011). A practical guide to evaluating colocalization in biological microscopy. Am J Physiol Cell Physiol *300*, C723-C742.

Farfel-Becker, T., Roney, J.C., Cheng, X.T., Li, S., Cuddy, S.R., and Sheng, Z.H. (2019). Neuronal Soma-Derived Degradative Lysosomes Are Continuously Delivered to Distal Axons to Maintain Local Degradation Capacity. Cell Rep *28*, 51-64.e54.

Fjorback, A.W., Seaman, M., Gustafsen, C., Mehmedbasic, A., Gokool, S., Wu, C., Militz, D., Schmidt, V., Madsen, P., Nyengaard, J.R.*, et al.* (2012). Retromer binds the FANSHY sorting motif in SorLA to regulate amyloid precursor protein sorting and processing. The Journal of neuroscience : the official journal of the Society for Neuroscience *32*, 1467-1480.

Ginsberg, S.D., Malek-Ahmadi, M.H., Alldred, M.J., Chen, Y., Chen, K., Chao, M.V., Counts, S.E., and Mufson, E.J. (2019). Brain-derived neurotrophic factor (BDNF) and TrkB hippocampal gene expression are putative predictors of neuritic plaque and neurofibrillary tangle pathology. Neurobiology of Disease *132*, 104540.

744 Glerup, S., Lume, M., Olsen, D., Nyengaard, J.R., Vaegter, C.B., Gustafsen, C., Christensen, E.I.,
745 Kjolby, M., Hay-Schmidt, A., Bender, D.*, et al.* (2013). SorLA controls neurotrophic activity by
746 sorting of GDNF and its receptors GFRalpha1 and RET. Cell Rep *3*, 186-199.
747 Gowrishankar, S., Yuan, P., Wu, Y., Schrag, M., Paradise, S., Grutzendler, J., De Camilli, P., and
748 Ferguson, S.M. (2015). Massive accumulation of luminal protease-deficient axonal lysosomes at
749 Alzheimer's disease amyloid plaques. Proceedings of the National Academy of Sciences *112*,
750 E3699-E3708.
751 Grant, B.D., and Donaldson, J.G. (2009). Pathways and mechanisms of endocytic recycling. Nat
752 Rev Mol Cell Biol *10*, 597-608.
753 Hamasaki, M., Araki, N., and Hatae, T. (2004). Association of early endosomal autoantigen 1 with
754 macropinocytosis in EGF-stimulated A431 cells. Anat Rec A Discov Mol Cell Evol Biol *277*, 298-
755 306.
756 Herskowitz, J.H., Offe, K., Deshpande, A., Kahn, R.A., Levey, A.I., and Lah, J.J. (2012). GGA1-
757 mediated endocytic traffic of LR11/SorLA alters APP intracellular distribution and amyloid-beta
758 production. Mol Biol Cell *23*, 2645-2657.
759 Hojland, A., Richner, M., Molgaard, S., Dieu, R.S., Eskelund, A., Nykjaer, A., Nyengaard, J.R.,
760 Lykkesfeldt, J., Glerup, S., and Nielsen, M.S. (2018). Biochemical and cognitive effects of
761 docosahexaenoic acid differ in a developmental and SorLA dependent manner. Behav Brain Res
762 *348*, 90-100.
763 Holstege, H., van der Lee, S.J., Hulsman, M., Wong, T.H., van Rooij, J.G., Weiss, M.,
764 Louwersheimer, E., Wolters, F.J., Amin, N., Uitterlinden, A.G.*, et al.* (2017). Characterization of
765 pathogenic SORL1 genetic variants for association with Alzheimer's disease: a clinical
766 interpretation strategy. Eur J Hum Genet *25*, 973-981.
767 Huang, T.Y., Zhao, Y., Jiang, L.L., Li, X., Liu, Y., Sun, Y., Pina-Crespo, J.C., Zhu, B., Masliah, E.,
768 Willnow, T.E.*, et al.* (2017). SORLA attenuates EphA4 signaling and amyloid beta-induced
769 neurodegeneration. J Exp Med *214*, 3669-3685.
770 Huang, T.Y., Zhao, Y., Li, X., Wang, X., Tseng, I.C., Thompson, R., Tu, S., Willnow, T.E., Zhang, Y.W.,
771 and Xu, H. (2016). SNX27 and SORLA Interact to Reduce Amyloidogenic Subcellular Distribution
772 and Processing of Amyloid Precursor Protein. The Journal of neuroscience : the official journal of
773 the Society for Neuroscience *36*, 7996-8011.
774 Huang, Z., Shimazu, K., Woo, N.H., Zang, K., Muller, U., Lu, B., and Reichardt, L.F. (2006). Distinct
775 roles of the beta 1-class integrins at the developing and the mature hippocampal excitatory
776 synapse. The Journal of neuroscience : the official journal of the Society for Neuroscience *26*,
777 11208-11219.
778 Hung, C., Tuck, E., Stubbs, V., van der Lee, S.J., Aalfs, C., van Spaendonk, R., Scheltens, P., Hardy,
779 J., Holstege, H., and Livesey, F.J. (2021). SORL1 deficiency in human excitatory neurons causes
780 APP-dependent defects in the endolysosome-autophagy network. Cell Rep *35*, 109259.
781 Hwang, J., Estick, C.M., Ikonne, U.S., Butler, D., Pait, M.C., Elliott, L.H., Ruiz, S., Smith, K.,
782 Rentschler, K.M., Mundell, C.*, et al.* (2019). The Role of Lysosomes in a Broad Disease-Modifying
783 Approach Evaluated across Transgenic Mouse Models of Alzheimer's Disease and Parkinson's
784 Disease and Models of Mild Cognitive Impairment. Int J Mol Sci *20*.
785 Karch, C.M., and Goate, A.M. (2015). Alzheimer's disease risk genes and mechanisms of disease
786 pathogenesis. Biol Psychiatry *77*, 43-51.

787 Klinger, S.C., Siupka, P., and Nielsen, M.S. (2015). Retromer-Mediated Trafficking of
788 Transmembrane Receptors and Transporters. Membranes (Basel) *5*, 288-306.
789 Knupp, A., Mishra, S., Martinez, R., Braggin, J.E., Szabo, M., Kinoshita, C., Hailey, D.W., Small, S.A.,
790 Jayadev, S., and Young, J.E. (2020). Depletion of the AD Risk Gene SORL1 Selectively Impairs
791 Neuronal Endosomal Traffic Independent of Amyloidogenic APP Processing. Cell Rep *31*, 107719.
792 Koopmans, F., van Nierop, P., Andres-Alonso, M., Byrnes, A., Cijsouw, T., Coba, M.P., Cornelisse,
793 L.N., Farrell, R.J., Goldschmidt, H.L., Howrigan, D.P.*, et al.* (2019). SynGO: An Evidence-Based,
794 Expert-Curated Knowledge Base for the Synapse. Neuron *103*, 217-234 e214.
795 Kwart, D., Gregg, A., Scheckel, C., Murphy, E.A., Paquet, D., Duffield, M., Fak, J., Olsen, O., Darnell,
796 R.B., and Tessier-Lavigne, M. (2019). A Large Panel of Isogenic APP and PSEN1 Mutant Human
797 iPSC Neurons Reveals Shared Endosomal Abnormalities Mediated by APP beta-CTFs, Not Abeta.
798 Neuron *104*, 256-270 e255.
799 Lambert, J.C., Ibrahim-Verbaas, C.A., Harold, D., Naj, A.C., Sims, R., Bellenguez, C., Jun, G.,
800 Destefano, A.L., Bis, J.C., Beecham, G.W.*, et al.* (2013). Meta-analysis of 74,046 individuals
801 identifies 11 new susceptibility loci for Alzheimer's disease. Nat Genet *45*, 1452-1458.
802 Leek, J.T., Johnson, W.E., Parker, H.S., Jaffe, A.E., and Storey, J.D. (2012). The sva package for
803 removing batch effects and other unwanted variation in high-throughput experiments.
804 Bioinformatics *28*, 882-883.
805 Levy, S., Sutton, G., Ng, P.C., Feuk, L., Halpern, A.L., Walenz, B.P., Axelrod, N., Huang, J., Kirkness,
806 E.F., Denisov, G.*, et al.* (2007). The diploid genome sequence of an individual human. PLoS Biol *5*,
807 e254.
808 Li, B., and Dewey, C.N. (2011). RSEM: accurate transcript quantification from RNA-Seq data with
809 or without a reference genome. BMC Bioinformatics *12*, 323.
810 Lorenzen, A., Samosh, J., Vandewark, K., Anborgh, P.H., Seah, C., Magalhaes, A.C., Cregan, S.P.,
811 Ferguson, S.S.G., and Pasternak, S.H. (2010). Rapid and Direct Transport of Cell Surface APP to
812 the Lysosome defines a novel selective pathway. Molecular Brain *3*, 11.
813 Mallard, F., Antony, C., Tenza, D., Salamero, J., Goud, B., and Johannes, L. (1998). Direct pathway
814 from early/recycling endosomes to the Golgi apparatus revealed through the study of shiga toxin
815 B-fragment transport. J Cell Biol *143*, 973-990.
816 Manders, E., Verbeek, F., and Aten, J. (1993). Measurement of co-localization of objects in dual-
817 colour confocal images. Journal of microscopy *169*, 375-382.
818 Marsh, E.W., Leopold, P.L., Jones, N.L., and Maxfield, F.R. (1995). Oligomerized transferrin
819 receptors are selectively retained by a lumenal sorting signal in a long-lived endocytic recycling
820 compartment. J Cell Biol *129*, 1509-1522.
821 Martin-Belmonte, A., Aguado, C., Alfaro-Ruiz, R., Itakura, M., Moreno-Martinez, A.E., de la Ossa,
822 L., Molnar, E., Fukazawa, Y., and Lujan, R. (2020). Age-Dependent Shift of AMPA Receptors From
823 Synapses to Intracellular Compartments in Alzheimer's Disease: Immunocytochemical Analysis of
824 the CA1 Hippocampal Region in APP/PS1 Transgenic Mouse Model. Front Aging Neurosci *12*,
825 577996.
826 Marwaha, R., and Sharma, M. (2017). DQ-Red BSA Trafficking Assay in Cultured Cells to Assess
827 Cargo Delivery to Lysosomes. Bio Protoc *7*.
828 Maxfield, F.R., and McGraw, T.E. (2004). Endocytic recycling. Nature reviews Molecular cell
829 biology *5*, 121-132.

830 Mayle, K.M., Le, A.M., and Kamei, D.T. (2012). The intracellular trafficking pathway of transferrin.
831 Biochim Biophys Acta *1820*, 264-281.
832 McQuin, C., Goodman, A., Chernyshev, V., Kamentsky, L., Cimini, B.A., Karhohs, K.W., Doan, M.,
833 Ding, L., Rafelski, S.M., Thirstrup, D.*, et al.* (2018). CellProfiler 3.0: Next-generation image
834 processing for biology. PLOS Biology *16*, e2005970.
835 Offe, K., Dodson, S.E., Shoemaker, J.T., Fritz, J.J., Gearing, M., Levey, A.I., and Lah, J.J. (2006). The
836 lipoprotein receptor LR11 regulates amyloid beta production and amyloid precursor protein
837 traffic in endosomal compartments. The Journal of neuroscience : the official journal of the
838 Society for Neuroscience *26*, 1596-1603.
839 Olav M. Andersen, N.B., Anne M. Landau, Gro Grunnet Pløen, Anne Mette G. Jensen, Giulia
840 Monti, Benedicte Parm Ulhøi, Jens Randel Nyengaard, Kirsten Rosenmay Jacobsen, Margarita
841 Melnikova Jørgensen, Ida E. Holm, Marianne L. Kristensen, Esben Søvsø Szocska Hansen,
842 Charlotte E. Teunissen, Laura Breidenbach, Mathias Droescher, Ying Liu, Hanne Skovsgaard
843 Pedersen, Henrik Callesen, Yonglun Luo, Lars Bolund, David J. Brooks, Christoffer Laustsen, Scott
844 A. Small, Lars F. Mikkelsen, Charlotte B. Sørensen (2021). In vivo evidence that SORL1, encoding
845 the endosomal recycling receptor SORLA, can function as a causal gene in Alzheimer's Disease.
846 bioRxiv *doi: https://doi.org/10.1101/2021.07.13.452149*.
847 Ouellette, S.P., and Carabeo, R.A. (2010). A Functional Slow Recycling Pathway of Transferrin is
848 Required for Growth of Chlamydia. Front Microbiol *1*, 112.
849 Park, M., Penick, E.C., Edwards, J.G., Kauer, J.A., and Ehlers, M.D. (2004). Recycling endosomes
850 supply AMPA receptors for LTP. Science *305*, 1972-1975.
851 Patapoutian, A., and Reichardt, L.F. (2001). Trk receptors: mediators of neurotrophin action. Curr
852 Opin Neurobiol *11*, 272-280.
853 Pietila, M., Sahgal, P., Peuhu, E., Jantti, N.Z., Paatero, I., Narva, E., Al-Akhrass, H., Lilja, J.,
854 Georgiadou, M., Andersen, O.M.*, et al.* (2019). SORLA regulates endosomal trafficking and
855 oncogenic fitness of HER2. Nat Commun *10*, 2340.
856 Qureshi, Y.H., Patel, V.M., Berman, D.E., Kothiya, M.J., Neufeld, J.L., Vardarajan, B., Tang, M.,
857 Reyes-Dumeyer, D., Lantigua, R., Medrano, M.*, et al.* (2018). An Alzheimer's Disease-Linked Loss-
858 of-Function CLN5 Variant Impairs Cathepsin D Maturation, Consistent with a Retromer Trafficking
859 Defect. Mol Cell Biol *38*.
860 Racoosin, E.L., and Swanson, J.A. (1993). Macropinosome maturation and fusion with tubular
861 lysosomes in macrophages. J Cell Biol *121*, 1011-1020.
862 Raghavan, N.S., Brickman, A.M., Andrews, H., Manly, J.J., Schupf, N., Lantigua, R., Wolock, C.J.,
863 Kamalakaran, S., Petrovski, S., Tosto, G.*, et al.* (2018). Whole-exome sequencing in 20,197
864 persons for rare variants in Alzheimer's disease. Ann Clin Transl Neurol *5*, 832-842.
865 Ramilowski, J.A., Goldberg, T., Harshbarger, J., Kloppmann, E., Lizio, M., Satagopam, V.P., Itoh,
866 M., Kawaji, H., Carninci, P., Rost, B.*, et al.* (2015). A draft network of ligand-receptor-mediated
867 multicellular signalling in human. Nat Commun *6*, 7866.
868 Rapaport, D., Lugassy, Y., Sprecher, E., and Horowitz, M. (2010). Loss of SNAP29 Impairs Endocytic
869 Recycling and Cell Motility. PLOS ONE *5*, e9759.
870 Ren, M., Xu, G., Zeng, J., De Lemos-Chiarandini, C., Adesnik, M., and Sabatini, D.D. (1998).
871 Hydrolysis of GTP on rab11 is required for the direct delivery of transferrin from the pericentriolar
872 recycling compartment to the cell surface but not from sorting endosomes. Proc Natl Acad Sci U
873 S A *95*, 6187-6192.

874 Rogaeva, E., Meng, Y., Lee, J.H., Gu, Y., Kawarai, T., Zou, F., Katayama, T., Baldwin, C.T., Cheng,
875 R., Hasegawa, H.*, et al.* (2007a). The neuronal sortilin-related receptor SORL1 is genetically
876 associated with Alzheimer disease. Nat Genet.
877 Rogaeva, E., Meng, Y., Lee, J.H., Gu, Y., Kawarai, T., Zou, F., Katayama, T., Baldwin, C.T., Cheng,
878 R., Hasegawa, H.*, et al.* (2007b). The neuronal sortilin-related receptor SORL1 is genetically
879 associated with Alzheimer disease. Nat Genet *39*, 168-177.
880 Rohe, M., Hartl, D., Fjorback, A.N., Klose, J., and Willnow, T.E. (2013). SORLA-mediated trafficking
881 of TrkB enhances the response of neurons to BDNF. PLoS One *8*, e72164.
882 Romano, R., Rivellini, C., De Luca, M., Tonlorenzi, R., Beli, R., Manganelli, F., Nolano, M., Santoro,
883 L., Eskelinen, E.-L., Previtali, S.C.*, et al.* (2021). Alteration of the late endocytic pathway in
884 Charcot–Marie–Tooth type 2B disease. Cellular and Molecular Life Sciences *78*, 351-372.
885 Scheltens, P., De Strooper, B., Kivipelto, M., Holstege, H., Chetelat, G., Teunissen, C.E., Cummings,
886 J., and van der Flier, W.M. (2021). Alzheimer's disease. Lancet *397*, 1577-1590.
887 Schindelin, J., Arganda-Carreras, I., Frise, E., Kaynig, V., Longair, M., Pietzsch, T., Preibisch, S.,
888 Rueden, C., Saalfeld, S., Schmid, B.*, et al.* (2012). Fiji: an open-source platform for biological-
889 image analysis. Nat Methods *9*, 676-682.
890 Schmidt, V., Sporbert, A., Rohe, M., Reimer, T., Rehm, A., Andersen, O.M., and Willnow, T.E.
891 (2007). SorLA/LR11 regulates processing of amyloid precursor protein via interaction with
892 adaptors GGA and PACS-1. J Biol Chem *282*, 32956-32964.
893 Seaman, M.N. (2004). Cargo-selective endosomal sorting for retrieval to the Golgi requires
894 retromer. J Cell Biol *165*, 111-122.
895 Seaman, M.N. (2012). The retromer complex - endosomal protein recycling and beyond. J Cell Sci
896 *125*, 4693-4702.
897 Selkoe, D.J. (2002). Alzheimer's disease is a synaptic failure. Science *298*, 789-791.
898 Shi, Y., Kirwan, P., Smith, J., Robinson, H.P., and Livesey, F.J. (2012). Human cerebral cortex
899 development from pluripotent stem cells to functional excitatory synapses. Nat Neurosci *15*, 477-
900 486, S471.
901 Simoes, S., Neufeld, J.L., Triana-Baltzer, G., Moughadam, S., Chen, E.I., Kothiya, M., Qureshi, Y.H.,
902 Patel, V., Honig, L.S., Kolb, H.*, et al.* (2020). Tau and other proteins found in Alzheimer's disease
903 spinal fluid are linked to retromer-mediated endosomal traffic in mice and humans. Science
904 translational medicine *12*.
905 Simoes S., G.J., Buitrago L., Qureshi Y.H., Feng X., Kothiya M., Cortes E., Patel V., Kannan S., Kim
906 Y.-H., Chang K.-T., ADNI, Hussaini A., Moreno H., Di Paolo G., Andersen O.M., Small S.A (2021).
907 Alzheimer’s vulnerable brain region relies on a distinct retromer core dedicated to endosomal
908 recycling. . Cell Reports *Accepted*.
909 Small, S.A., and Gandy, S. (2006). Sorting through the cell biology of Alzheimer's disease:
910 intracellular pathways to pathogenesis. Neuron *52*, 15-31.
911 Small, S.A., and Petsko, G.A. (2020). Endosomal recycling reconciles the Alzheimer's disease
912 paradox. Science translational medicine *12*.
913 Sonnichsen, B., De Renzis, S., Nielsen, E., Rietdorf, J., and Zerial, M. (2000). Distinct membrane
914 domains on endosomes in the recycling pathway visualized by multicolor imaging of Rab4, Rab5,
915 and Rab11. J Cell Biol *149*, 901-914.
916 Spoelgen, R., von Arnim, C.A., Thomas, A.V., Peltan, I.D., Koker, M., Deng, A., Irizarry, M.C.,
917 Andersen, O.M., Willnow, T.E., and Hyman, B.T. (2006). Interaction of the cytosolic domains of

sorLA/LR11 with the amyloid precursor protein (APP) and beta-secretase beta-site APP-cleaving enzyme. The Journal of neuroscience : the official journal of the Society for Neuroscience *26*, 418-428.

Sun, J., and Roy, S. (2018). The physical approximation of APP and BACE-1: A key event in alzheimer's disease pathogenesis. Dev Neurobiol *78*, 340-347.

Temkin, P., Morishita, W., Goswami, D., Arendt, K., Chen, L., and Malenka, R. (2017). The Retromer Supports AMPA Receptor Trafficking During LTP. Neuron *94*, 74-82 e75.

Thonberg, H., Chiang, H.H., Lilius, L., Forsell, C., Lindstrom, A.K., Johansson, C., Bjorkstrom, J., Thordardottir, S., Sleegers, K., Van Broeckhoven, C*., et al.* (2017). Identification and description of three families with familial Alzheimer disease that segregate variants in the SORL1 gene. Acta Neuropathol Commun *5*, 43.

Tian, X., Gala, U., Zhang, Y., Shang, W., Nagarkar Jaiswal, S., di Ronza, A., Jaiswal, M., Yamamoto, S., Sandoval, H., Duraine, L*., et al.* (2015). A Voltage-Gated Calcium Channel Regulates Lysosomal Fusion with Endosomes and Autophagosomes and Is Required for Neuronal Homeostasis. PLOS Biology *13*, e1002103.

Wakabayashi, K., Narisawa-Saito, M., Iwakura, Y., Arai, T., Ikeda, K., Takahashi, H., and Nawa, H. (1999). Phenotypic down-regulation of glutamate receptor subunit GluR1 in Alzheimer's disease. Neurobiol Aging *20*, 287-295.

Wang, Y., Eng, D.G., Kaverina, N.V., Loretz, C.J., Koirala, A., Akilesh, S., Pippin, J.W., and Shankland, S.J. (2020). Global transcriptomic changes occur in aged mouse podocytes. Kidney Int *98*, 1160-1173.

Willnow, T.E., and Andersen, O.M. (2013). Sorting receptor SORLA--a trafficking path to avoid Alzheimer disease. J Cell Sci *126*, 2751-2760.

Yap, C.C., Digilio, L., McMahon, L.P., Garcia, A.D.R., and Winckler, B. (2018). Degradation of dendritic cargos requires Rab7-dependent transport to somatic lysosomes. Journal of Cell Biology *217*, 3141-3159.

Yasuda, R.P., Ikonomovic, M.D., Sheffield, R., Rubin, R.T., Wolfe, B.B., and Armstrong, D.M. (1995). Reduction of AMPA-selective glutamate receptor subunits in the entorhinal cortex of patients with Alzheimer's disease pathology: a biochemical study. Brain Res *678*, 161-167.

Young, J.E., Boulanger-Weill, J., Williams, D.A., Woodruff, G., Buen, F., Revilla, A.C., Herrera, C., Israel, M.A., Yuan, S.H., Edland, S.D*., et al.* (2015). Elucidating Molecular Phenotypes Caused by the SORL1 Alzheimer's Disease Genetic Risk Factor Using Human Induced Pluripotent Stem Cells. Cell stem cell *16*, 373-385.

Yuan, S.H., Martin, J., Elia, J., Flippin, J., Paramban, R.I., Hefferan, M.P., Vidal, J.G., Mu, Y., Killian, R.L., Israel, M.A*., et al.* (2011). Cell-surface marker signatures for the isolation of neural stem cells, glia and neurons derived from human pluripotent stem cells. PLoS One *6*, e17540.

Zigdon, H., Meshcheriakova, A., Farfel-Becker, T., Volpert, G., Sabanay, H., and Futerman, A.H. (2017). Altered lysosome distribution is an early neuropathological event in neurological forms of Gaucher disease. FEBS Lett *591*, 774-783.

**Figure legends**

**Figure 1.** Loss of *SORL1* expression leads to increased TRKB and GLUA1 localization in early endosomes. Representative immunofluorescent images of WT and *SORL1*KO neurons showing increased colocalization of **(a)** TRKB (green) and **(b)** GLUA1 (green) with EEA1 (red). All neurons were immunolabeled with MAP2 (far-red) and counterstained with DAPI (blue). Scale bar: 10μm. In all cases, quantification of colocalization was represented as Mander's correlation co-efficient (MCC). 1 WT and 2 *SORL1*KO isogenic clones were used for these experiments and 10 images per clone per genotype were analyzed. Data represented as mean ± SD. Data was analyzed using parametric two-tailed unpaired t test. Significance was defined as a value of *$p < 0.05$, **$p < 0.01$, ***$p < 0.001$, and ****$p < 0.0001$.

**Figure 2.** Loss of *SORL1* expression impairs trafficking to late endosomes and lysosomes.
**a)** *SORL1*KO neurons show reduced lysosomal proteolytic activity as measured by DQ Red BSA. Representative immunofluorescent images of WT and *SORL1*KO neurons showing double immunolabeling for MAP2 (green) and DQ Red BSA (red). Scale bar: 10μm Quantification of fluorescence intensity of DQ Red BSA using ImageJ software. **(b-f)** *SORL1*KO neurons show reduced colocalization of cargo with late endosomes and lysosomes. Representative immunofluorescent images of WT and *SORL1*KO neurons showing reduced colocalization of **(b)** TRKB (green) and **(c)** GLUA1 (green) with Rab7 positive late endosomes (red) in *SORL1*KO neurons. Representative immunofluorescent images of WT and *SORL1*KO neurons showing reduced colocalization of **(d)** APP (green) and **(e)** TRKB (green) and **(f)** GLUA1 (green) with LAMP1 positive lysosomes (red) in *SORL1*KO neurons. Scale bar: 10μm. In all cases, quantification of colocalization was represented as Mander's correlation co-efficient (MCC). 1 WT and 2 *SORL1*KO isogenic clones were used for these experiments and 10 images per clone per genotype were analyzed. Data represented as mean ± SD. Data was analyzed using parametric two-tailed unpaired t test. Significance was defined as a value of *$p < 0.05$, **$p < 0.01$, ***$p < 0.001$, and ****$p < 0.0001$.

**Figure 3:** Enhancing *SORL1* Expression improves trafficking to late endosomes and lysosomes

**a)** *SORL1*OE neurons show no change in lysosomal proteolytic activity as measured using DQ Red BSA after a 6 hour treatment but do show an enhancement of trafficking at 24 hours. Representative immunofluorescent images of WT and *SORL1*OE neurons showing double immunolabeling for MAP2 (green) and DQ Red BSA (red). Scale bar: 10 μm. Quantification of fluorescence intensity of DQ Red BSA using ImageJ software. 1 cell line of each genotype (WT vs. SORL1 OE) were used for these experiments. 10 images per genotype were analyzed. Representative immunofluorescent images of WT and *SORL1*OE neurons showing increased colocalization of APP, TRKB and GLUA1 (green) with Rab7 (red) **(b-d)** and LAMP1 (red) **(e-g)** in *SORL1*OE neurons. *SORL1*OE neurons and controls have endogenous GFP expression due to the piggybac vector system. GFP fluorescence is pseudo-colored (Far-red) and was used to outline cell bodies. Scale bar: 10μm. Nuclei are counterstained with DAPI (blue). In all cases, quantification of colocalization was represented as Mander's correlation co-efficient (MCC). 1 cell line of each genotype (WT vs. SORL1 OE) were used for these experiments. 10 images per genotype were analyzed. Data represented as mean ± SD. Data was analyzed using parametric two-tailed unpaired t test. Significance was defined as a value of *$p < 0.05$, **$p < 0.01$, ***$p < 0.001$, and ****$p < 0.0001$.

**Figure 4.** Loss of *SORL1* impacts the cell surface recycling pathway

**a)** *SORL1*KO neurons show slower rate of transferrin recycling. Quantification of fluorescence intensity of intracellular transferrin at different time points after treating cells with Alexa Fluor 647-conjugated transferrin for 15 mins, using ImageJ software. Data represented as percent of time 0 fluorescence intensity. 2 WT and 2 *SORL1*KO isogenic clones were used for these experiments. 12 images per clone per genotype were analyzed. **(b)** *SORL1*KO neurons show larger recycling endosomes. Representative immunofluorescent images of WT and *SORL1*KO neurons labeled with antibodies for MAP2 (red) and Rab11 (green). Nuclei were counterstained with DAPI (blue). Scale bar: 5μm. Quantification of size of Rab11 labeled recycling endosomes using CellProfiler software. 1 WT and 2 *SORL1*KO isogenic clones were used for these experiments. 15 images per clone per

genotype were analyzed. Representative immunofluorescent images of WT and *SORL1*KO neurons showing increased colocalization of **(c)** APP (green), **(d)** TRKB (green) and **(e)** GLUA1 (green) with Rab11 positive recycling endosomes (red) in *SORL1*KO neurons. Scale bar:10μm In all cases, quantification of colocalization was represented as Mander's correlation co-efficient (MCC). 1 WT and 2 *SORL1*KO isogenic clones were used for these experiments. 10 images per clone per genotype were analyzed. Data represented as mean ± SD. Data was analyzed using parametric two-tailed unpaired t test and two-was ANOVA. Significance was defined as a value of *p < 0.05, **p < 0.01, ***p < 0.001, and ****p < 0.0001.

**Figure 5.** Loss of *SORL1* expression impairs recycling to the cell surface.

**a-b)** *SORL1*KO neurons show reduced cell surface expression of APP **(a)** and GLUA1 **(b)**. Representative immunofluorescent images of WT and *SORL1*KO neurons labeled with antibodies for APP **(a)** (red) and GLUA1 **(b)** (red). Scale bar: 5μm. Intensity of APP and GLUA1 measured using ImageJ software. Data is presented as a ratio of surface intensity to total intensity. 2 WT and 2 *SORL1*KO clones were used in these experiments. 16 images per clone per genotype were analyzed. Data represented as mean ± SD. Normally distributed data was analyzed using parametric two-tailed unpaired t test. Significance was defined as a value of *p < 0.05, **p < 0.01, ***p < 0.001, and ****p < 0.0001. **(c)** Multielectrode array (MEA) analysis of WT and *SORL1*KO neurons at early (d27) and late (d66) time points of differentiation. 1 WT and 1 *SORL1*KO clone was used for these experiments. Data represented as mean ± SD. Data was analyzed using parametric two-tailed unpaired t test. Significance was defined as a value of *p < 0.05, **p < 0.01, ***p < 0.001, and ****p < 0.0001.

**Figure 6.** Overexpression of *SORL1* enhances endosomal recycling.

**a)** *SORL1*OE neurons show faster rate of transferrin recycling. Quantification of fluorescence intensity of intracellular transferrin at different time points after treating cells with Alexa Fluor 647-conjugated transferrin for 15 mins, using ImageJ software. Data represented as percent of time 0 fluorescence intensity. 1 cell line of each

genotype (WT vs. SORL1 OE) were used for these experiments. 10 images per genotype were analyzed. **(b)** *SORL1*OE neurons show reduced size of recycling endosomes. Representative immunofluorescent images of WT and *SORL1*OE neurons labeled with Rab11 (green) and MAP2 (red) showing smaller Rab11 positive recycling endosomes in *SORL1*OE neurons. Nuclei counterstained with DAPI (blue). Quantification of Rab11+ recycling endosome size performed using Cell Profiler software and represented as area of Rab11+ vesicles. Scale bar: 5μm. 1 cell line of each genotype (WT vs. SORL1 OE) were used for these experiments. 26 images per genotype were analyzed. Representative immunofluorescent images of WT and *SORL1*OE neurons showing increased colocalization of **(c)** APP (green), **(d)** TRKB (green) and **(e)** GLUA1 (green) with Rab11 (red) positive recycling endosomes. *SORL1*OE neurons and controls have endogenous GFP expression due to the piggybac vector system. GFP fluorescence is pseudo-colored (Far-red) and was used to outline cell bodies. Quantification of colocalization with Rab11 represented as Mander's Correlation Co-efficient (MCC). Scale bar: 10μm. 1 cell line of each genotype (WT vs. SORL1 OE) were used for these experiments. 10 images per genotype were analyzed. Representative immunofluorescent images of WT and *SORL1*OE neurons showing increased cell surface expression of **(f)** APP (red) and **(g)** GLUA1 (red) in *SORL1*OE neurons. Scale bar: 5μm Fluorescence intensity of APP and GLUA1 measured using ImageJ software. Data is presented as a ratio of surface intensity to total intensity. Nuclei counterstained with DAPI. 1 cell line of each genotype (WT vs. SORL1 OE) were used for these experiments. 12-14 images per genotype were analyzed. Data represented as mean ± SD. Data was analyzed using parametric two-tailed unpaired t test and two-way ANOVA. Significance defined as a value of *$p < 0.05$, **$p < 0.01$, ***$p < 0.001$, and ****$p < 0.0001$.

**Figure 7.** Analysis of bulk RNA-sequencing data indicates alterations in cell surface and extracellular trafficking, receptor-ligand and channel activity. Gene ontology analysis of DEGs in WT and *SORL1*KO neurons. Shown here are the top upregulated **(a)** and downregulated **(b)** molecular function terms in *SORL1*KO neurons. GO annotation terms are listed on the y-axis, adjusted p-value is shown on the x-axis. **(c)** Ligand-receptor network changes in *SORL1*KO neurons, identified if genes are more than 1.5-fold increased or decreased in *SORL1*KO

neurons with an adjusted p-value less than 0.05. Circles denote ligands, squares denote receptors, blue indicates genes expressed significantly lower in *SORL1*KO neurons, red indicates genes expressed significantly higher in *SORL1*KO neurons. Arrows point from ligand to receptor, denoting receptor-ligand interactions. Black arrows denote consistent expression changes between ligand and receptor, indicating that both genes in the pair are either upregulated or downregulated. Gray arrows denote inconsistent changes between ligand and receptor. Clusters impacted by cell surface recycling (β-integrins, ephrins) or neurotrophic signaling (FGF/FGFR, NGF/NGFR) are indicated by green dotted arrows. RNA was collected from 3 separate differentiations including a combination of two WT clones and two *SORL1*KO clones. Each sample includes 2-3 technical replicates.

**Figure 8. Model of modulation of SORL1 expression in hiPSC-derived cortical neurons.**

Modulation of SORLA expression regulates endosomal recycling and degradative pathways in hiPSC-derived neurons: The early endosome is a sorting hub where various cargo can be trafficked to degradative or cell surface recycling pathways in neurons (A). In this study, we mapped trafficking of three important neuronal cargo under conditions of depletion (B) or enhancement (C) of the AD risk gene SORL1/SORLA. As depicted in panel B, our data suggest that modulation of SORL1 expression significantly impacts the neuronal recycling pathway as we observe increased size and accumulation of cargo in recycling endosomes in SORL1 KO neurons compared to isogenic WT cells. Specifically, loss of SORL1 impacts recycling to the cell surface because, while there is increased cargo in recycling endosomes, there is a reduction of this cargo on the neuronal surface. Loss of SORL1 also impacts the degradative pathway out of the early endosome as there is a reduction of cargo in late endosome and lysosomes. As depicted in panel C, enhancement of SORL1 expression reciprocally impacts these pathways. SORL1 OE neurons also have an increase in cargo in recycling endosomes, but unlike KO cells, this results in more cell surface trafficking of neuronal cargo, leading to reduced stress (small size) of recycling endosomes. Additionally, SORL1 OE enhances trafficking out of the early endosome towards the degradative pathway as well. Taken together, our data solidifies the AD risk gene SORL1 as a key modulator of neuronal endosomal trafficking. Created with Biorender.com.

**Supplementary figures**

**Supplementary figure 1**.

Loss of *SORL1* expression leads to increased VPS35 localization in early endosomes. **(a)** Representative immunofluorescent images of WT and *SORL1*KO neurons showing increased colocalization of VPS35 (green) with EEA1 (red). All neurons were immunolabeled with MAP2 (far-red) and counterstained with DAPI (blue). Scale bar: 10μm. In all cases, quantification of colocalization was represented as Mander's correlation co-efficient (MCC). 1 WT and 2 SORL1KO isogenic clones were used for these experiments and 10 images per clone per genotype were analyzed. Data represented as mean ± SD. Significance was determined using parametric two-tailed unpaired t test and was defined as a value of *$p < 0.05$, **$p < 0.01$, ***$p < 0.001$, and ****$p < 0.0001$.

**Supplementary figure 2**

**a)** *SORL1*KO neurons show larger lysosome size and increased lysosome number. Representative immunofluorescent images of WT and *SORL1*KO neurons labeled with LAMP1 (green) and MAP2 (red) showing increased LAMP1 positive vesicle size in *SORL1*KO neurons. Quantification of LAMP1 size and number was performed using Cell Profiler software. LAMP1 size is represented as area of LAMP1 positive vesicles, and LAMP1 number is represented as number of LAMP1 positive vesicles per square micron of cell area. Scale bar: 5μm **(b)** *SORL1*KO neurons show no change in colocalization of lysosomes with the lysosomal enzyme Cathepsin D. Representative immunofluorescent images of WT and *SORL1*KO neurons labeled with antibodies for LAMP1 (green), Cathepsin D (red) and MAP2 (Far-red) showing no alteration in colocalization of Cathepsin-D with LAMP1 in *SORL1*KO neurons. Nuclei counterstained with DAPI (blue). Scale bar: 10μm Quantification of colocalization of LAMP1 with Cathepsin-D represented as Mander's correlation coefficient (MCC). 10-20 images were analyzed per genotype. Two isogenic clones of each genotype were used in all experiments. Data

represented as mean ± SD. Normally distributed data was analyzed using parametric two-tailed unpaired t test. Significance was defined as a value of *$p < 0.05$, **$p < 0.01$, ***$p < 0.001$, and ****$p < 0.0001$.

**Supplemental figure 3.**

Loss of SORL1 does not change protein expression of the compartments or cargo analyzed in this study as analyzed by Western blot. Representative blots in (a), quantification in (b).

**Supplemental figure 4**

**a)** Principal component analysis (PCA) plot of all RNAseq samples using all expressed genes. Samples are color coded by differentiation batch. Triangles represent WT samples, circles represent *SORL1*KO. Genotype accounts for the highest variance (37%, PC1, x-axis). **b)** Volcano plot. Log2 fold change between *SORL1*KO and WT is shown along the x-axis. Statistical significance is shown along the y-axis, and is measured by adjusted p-value. Genes upregulated in *SORL1*KO neurons are shown by red circles, genes downregulated in *SORL1*KO neurons are shown by blue circles. We observed 6643 DEGs, with 2819 upregulated and 3824 downregulated. There are significantly more down regulated genes than upregulated genes ($p<2.2e-16$). Grey circles represent genes that are not significantly differentially expressed.

**Supplemental figure 5 .**

Loss of *SORL1* expression alters synaptic pathways. Analysis of bulk RNA-sequencing data indicates alterations in synaptic pathway functioning. We conducted gene ontology analysis of DEGs in WT and *SORL1*KO neurons using the SynGO synaptic annotation database. Shown here are the top upregulated and biological process and cellular component terms in *SORL1*KO neurons. GO annotation terms are listed on the y-axis, adjusted p-value is shown on the x-axis. No downregulated pathways in the SynGO database were shown to be enriched in *SORL1*KO neurons.

## Supplemental Table 1.

Summary of statistical analyses for data presented in this manuscript. In this table we present the statistical data that correspond to the experiments presented in the figures. This includes the group means, the difference between the means ± SEM, and the 95% confidence interval.

Figure 1

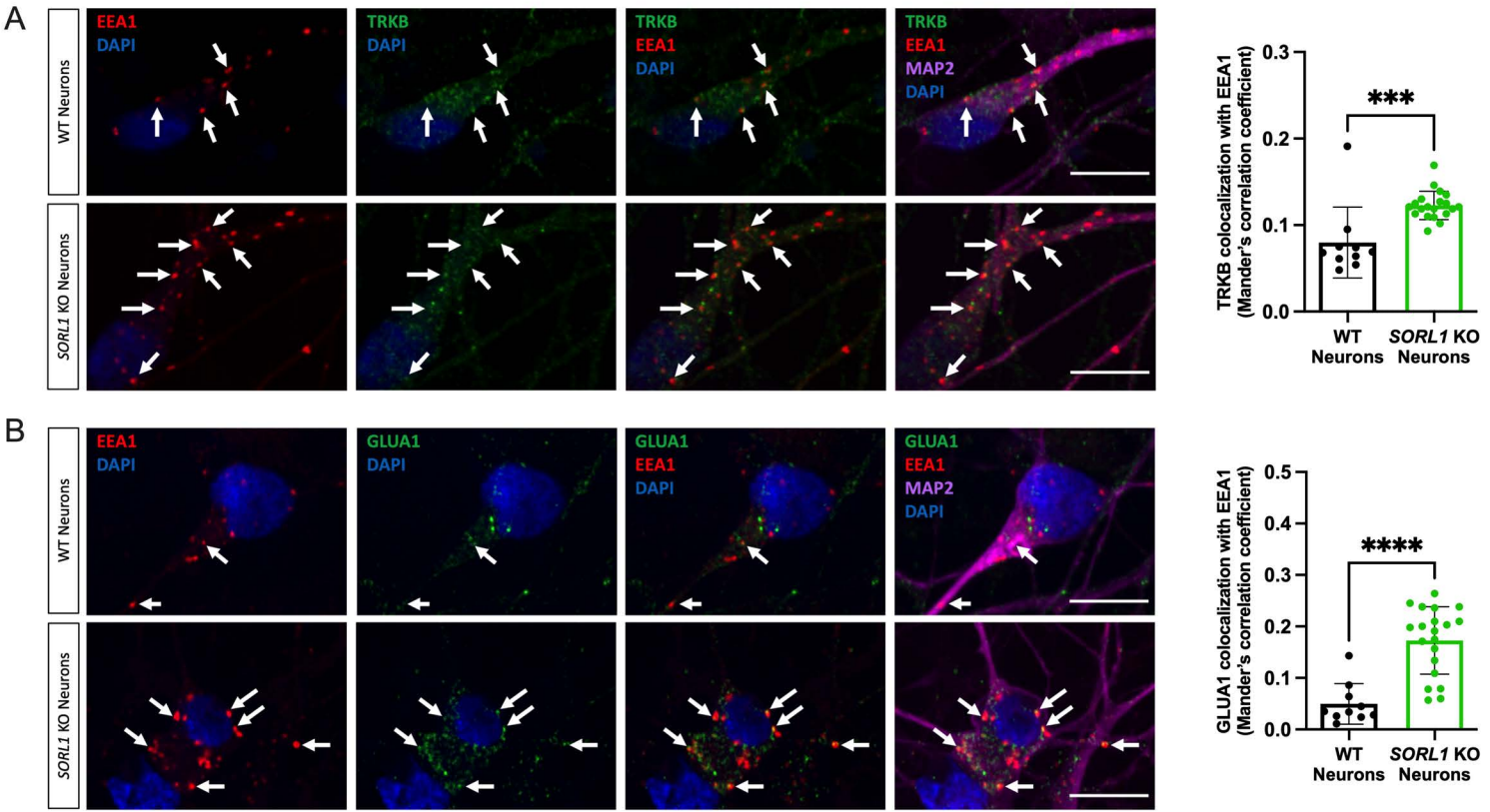
A
WT Neurons
SORL1 KO Neurons
EEA1
DAPI
TRKB
DAPI
TRKB
EEA1
DAPI
TRKB
EEA1
MAP2
DAPI
TRKB colocalization with EEA1
(Mander's correlation coefficient)
0.3
0.2
0.1
0.0
***
WT Neurons
SORL1 KO Neurons
B
WT Neurons
SORL1 KO Neurons
EEA1
DAPI
GLUA1
DAPI
GLUA1
EEA1
DAPI
GLUA1
EEA1
MAP2
DAPI
GLUA1 colocalization with EEA1
(Mander's correlation coefficient)
0.5
0.4
0.3
0.2
0.1
0.0
****
WT Neurons
SORL1 KO Neurons

Figure 2

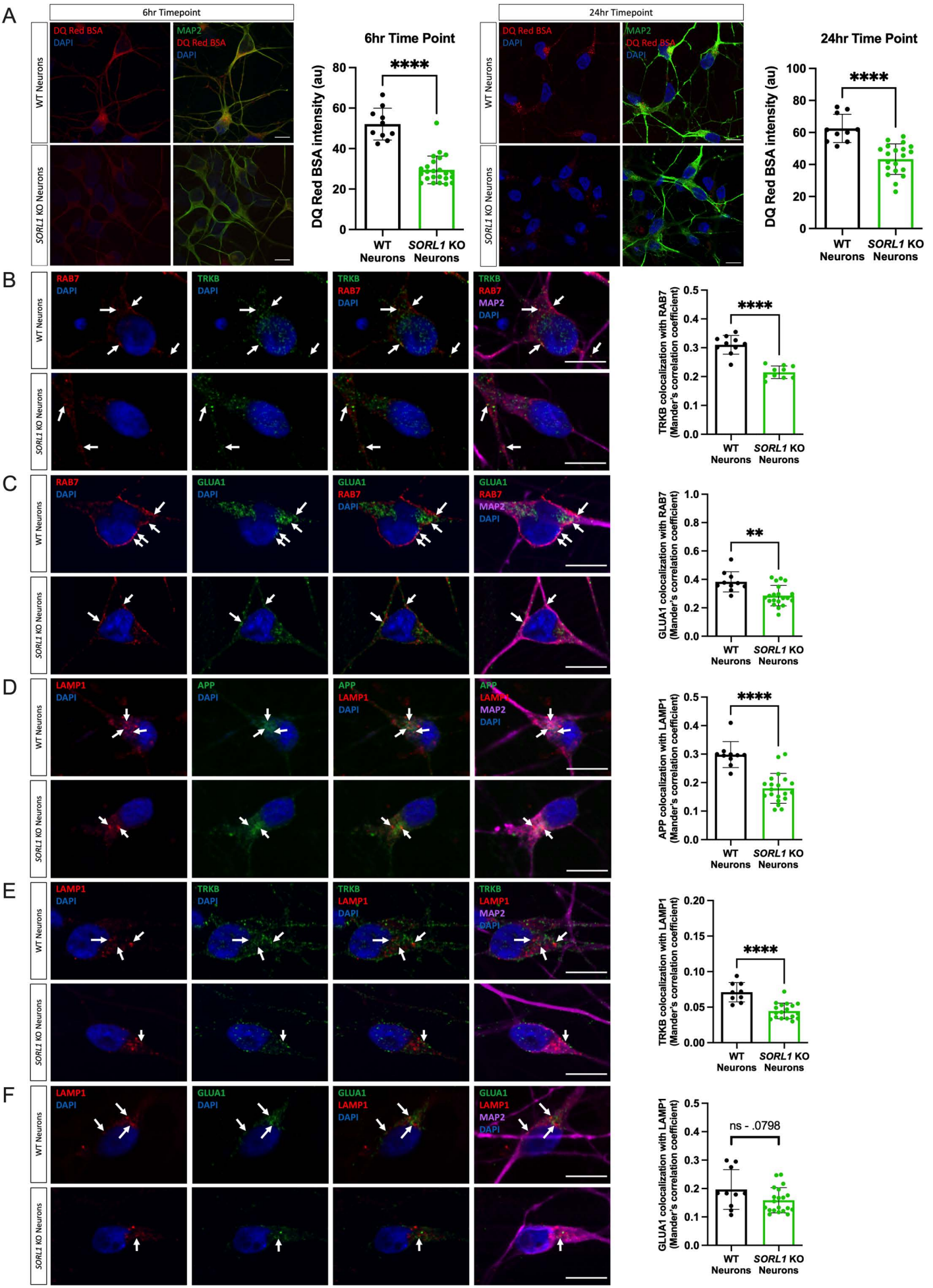
A
6hr Timepoint
24hr Timepoint
WT Neurons
SORL1 KO Neurons
DQ Red BSA
DAPI
MAP2
6hr Time Point
24hr Time Point
DQ Red BSA intensity (au)
****
WT Neurons
SORL1 KO Neurons
B
RAB7
TRKB
C
GLUA1
D
APP
LAMP1
E
F
TRKB colocalization with RAB7 (Mander's correlation coefficient)
GLUA1 colocalization with RAB7 (Mander's correlation coefficient)
APP colocalization with LAMP1 (Mander's correlation coefficient)
TRKB colocalization with LAMP1 (Mander's correlation coefficient)
GLUA1 colocalization with LAMP1 (Mander's correlation coefficient)
**
ns - .0798

# Figure 3

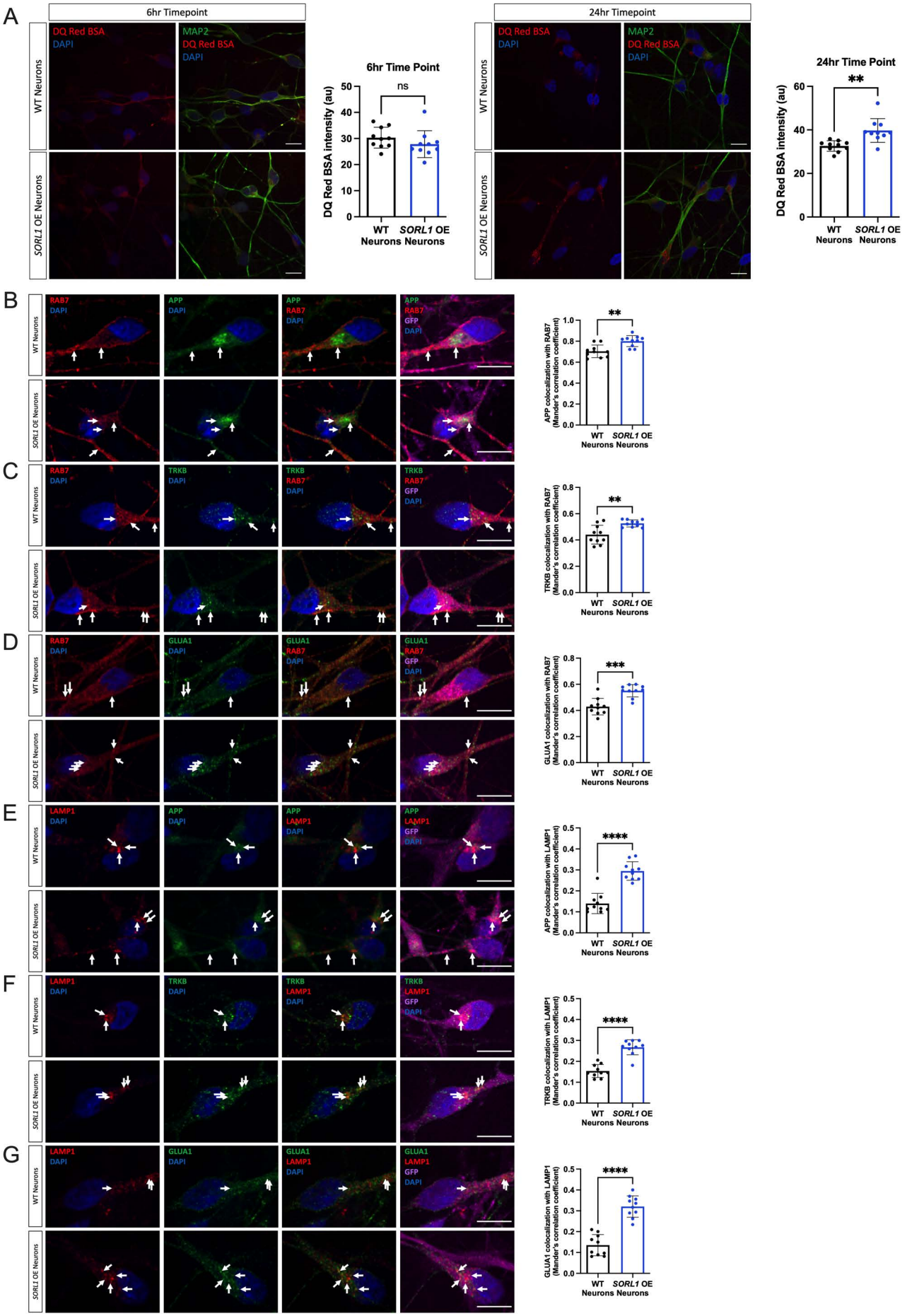
A
6hr Timepoint
24hr Timepoint
WT Neurons
SORL1 OE Neurons
DQ Red BSA
DAPI
MAP2
6hr Time Point
24hr Time Point
DQ Red BSA intensity (au)
ns
**
WT Neurons
SORL1 OE Neurons
B
RAB7
APP
GFP
APP colocalization with RAB7 (Mander's correlation coefficient)
C
TRKB
TRKB colocalization with RAB7 (Mander's correlation coefficient)
D
GLUA1
GLUA1 colocalization with RAB7 (Mander's correlation coefficient)
***
E
LAMP1
APP colocalization with LAMP1 (Mander's correlation coefficient)
****
F
TRKB colocalization with LAMP1 (Mander's correlation coefficient)
G
GLUA1 colocalization with LAMP1 (Mander's correlation coefficient)

Figure 4

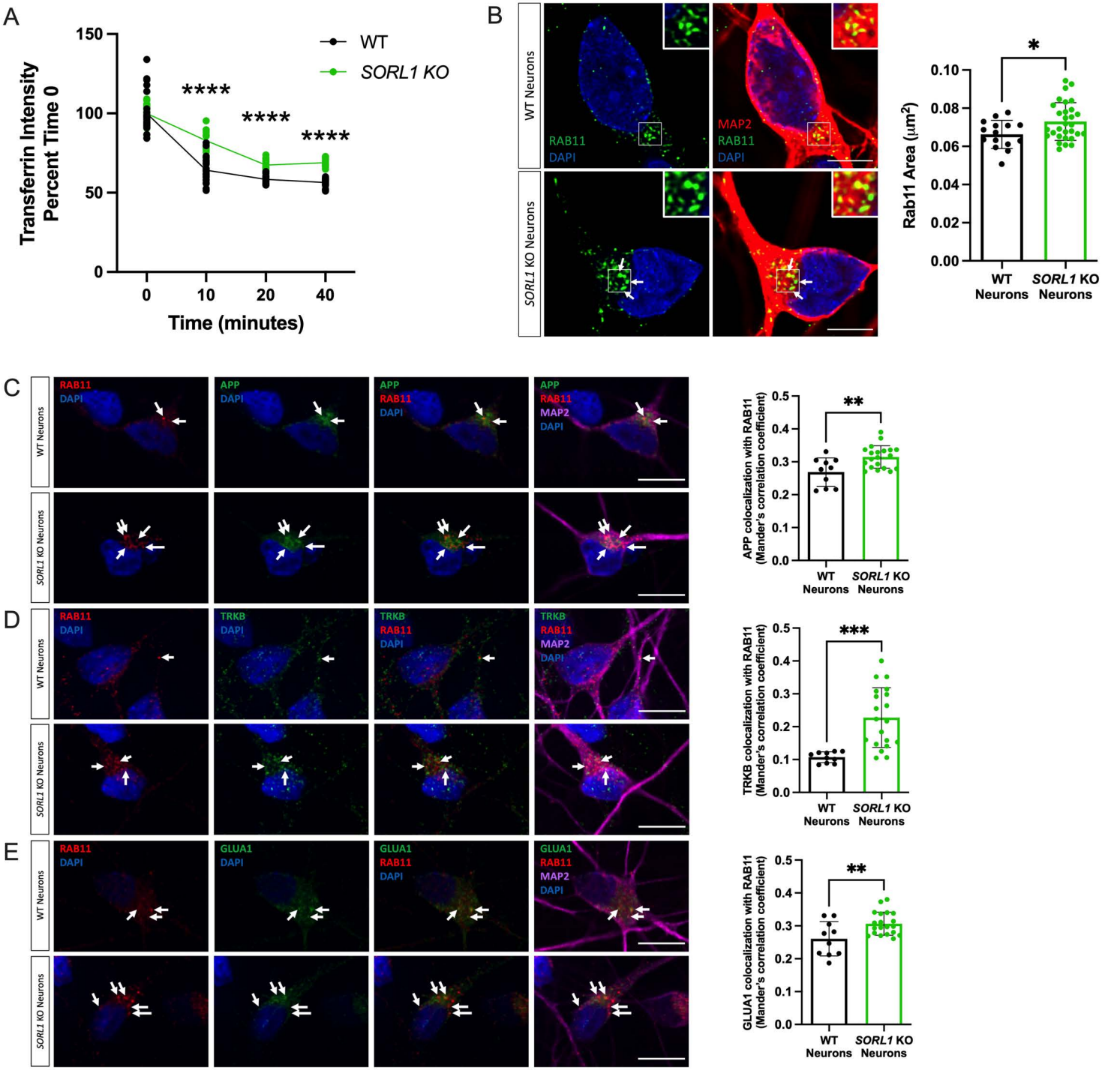
A
Transferrin Intensity Percent Time 0
Time (minutes)
WT
SORL1 KO
****
B
WT Neurons
SORL1 KO Neurons
RAB11
DAPI
MAP2
Rab11 Area (μm²)
C
APP
D
TRKB
E
GLUA1
APP colocalization with RAB11 (Mander's correlation coefficient)
TRKB colocalization with RAB11 (Mander's correlation coefficient)
GLUA1 colocalization with RAB11 (Mander's correlation coefficient)

Figure 5

A

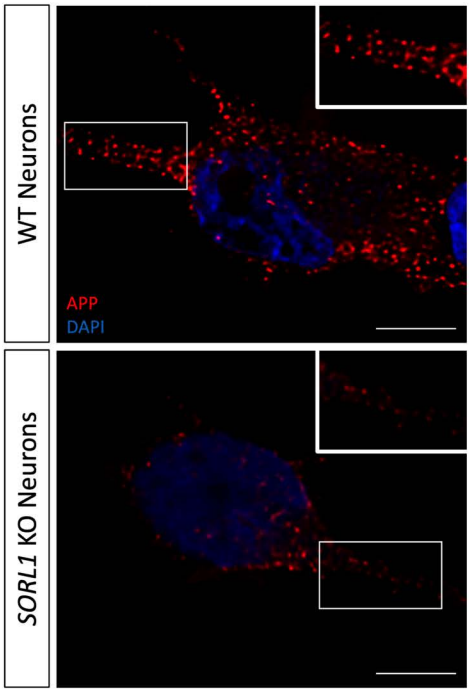
WT Neurons
APP
DAPI
SORL1 KO Neurons

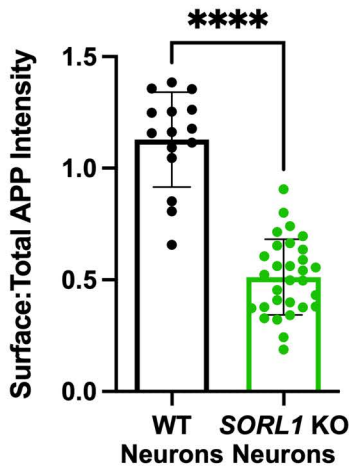
****
Surface:Total APP Intensity
1.5
1.0
0.5
0.0
WT Neurons
SORL1 KO Neurons

B

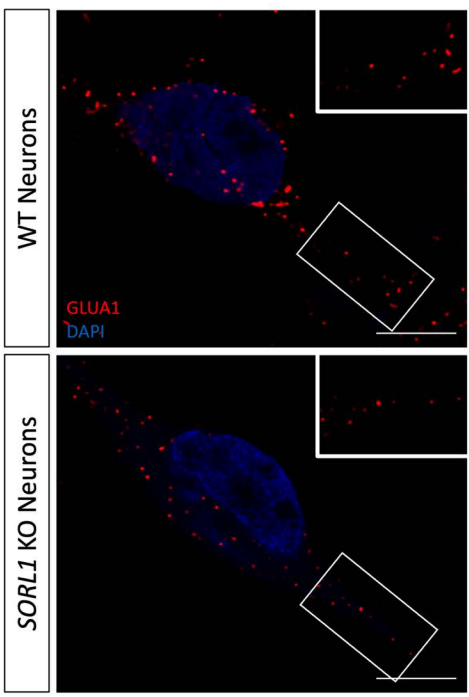
WT Neurons
GLUA1
DAPI
SORL1 KO Neurons

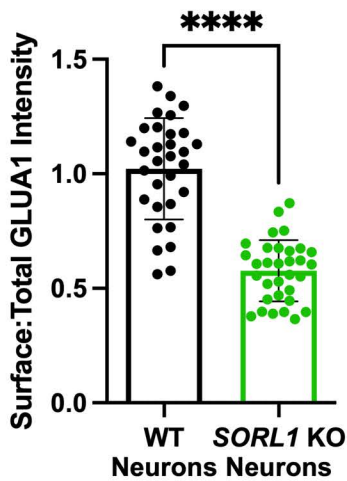
****
Surface:Total GLUA1 Intensity
1.5
1.0
0.5
0.0
WT Neurons
SORL1 KO Neurons

C

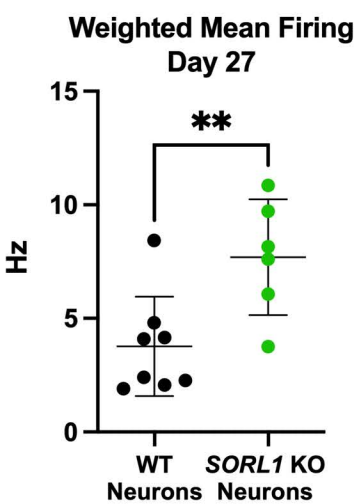
Weighted Mean Firing
Day 27
**
Hz
15
10
5
0
WT Neurons
SORL1 KO Neurons

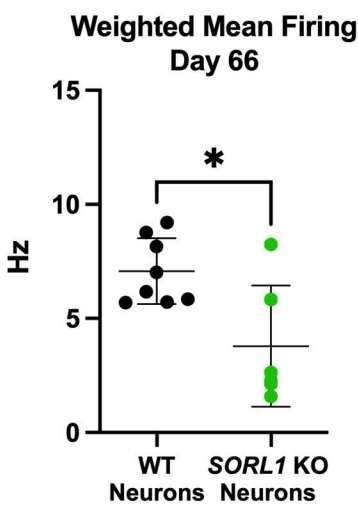
Weighted Mean Firing
Day 66
*
Hz
15
10
5
0
WT Neurons
SORL1 KO Neurons

Figure 6

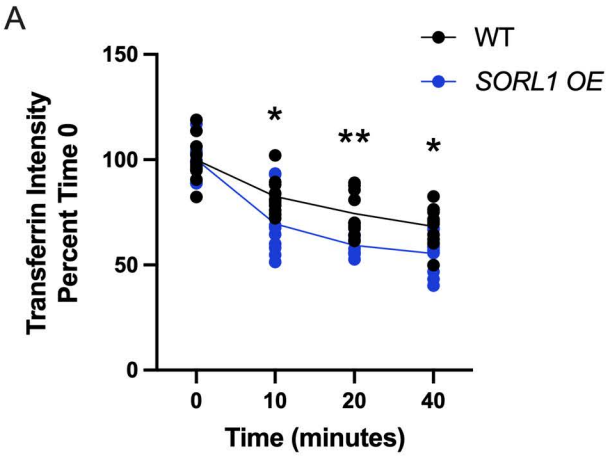
A
WT
SORL1 OE
Transferrin Intensity Percent Time 0
150
100
50
0
*
**
*
0
10
20
40
Time (minutes)

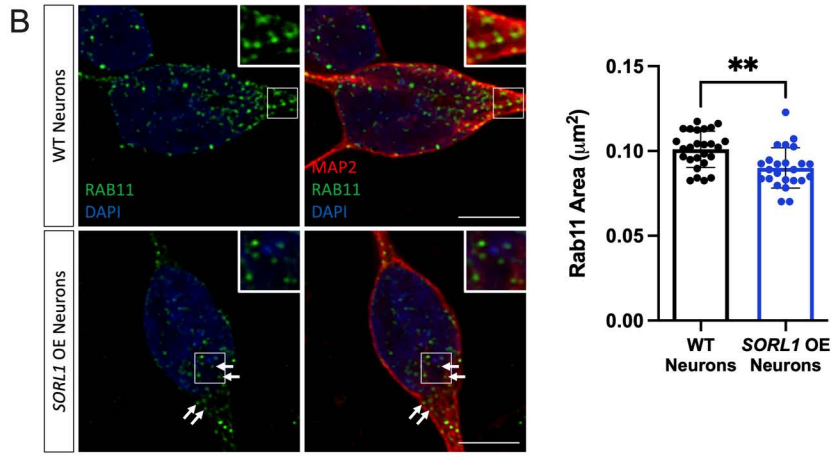
B
WT Neurons
SORL1 OE Neurons
RAB11
DAPI
MAP2
RAB11
DAPI
Rab11 Area (μm²)
0.15
0.10
0.05
0.00
**
WT Neurons
SORL1 OE Neurons

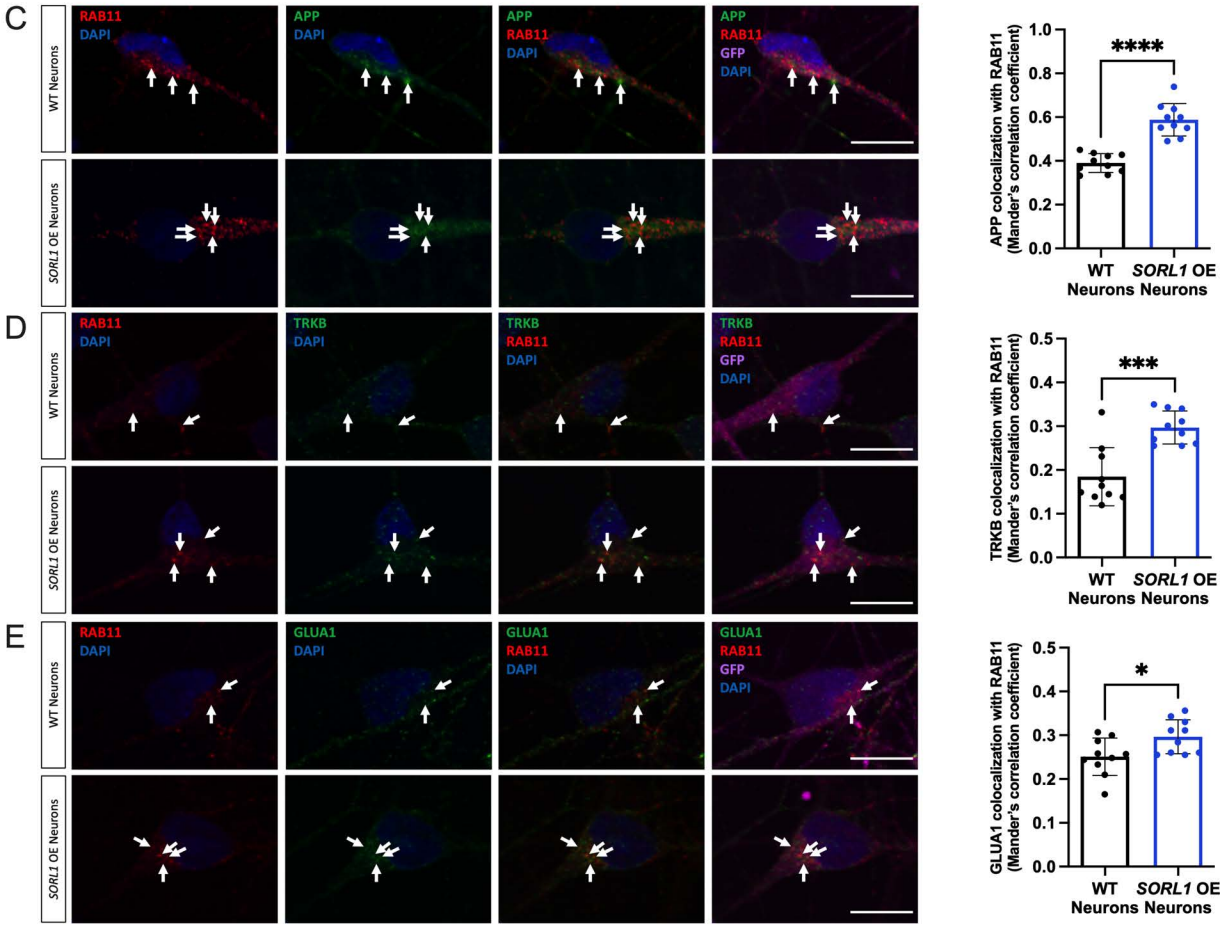
C
WT Neurons
SORL1 OE Neurons
RAB11
DAPI
APP
DAPI
APP
RAB11
DAPI
APP
RAB11
GFP
DAPI
APP colocalization with RAB11 (Mander's correlation coefficient)
1.0
0.8
0.6
0.4
0.2
0.0
****
WT Neurons
SORL1 OE Neurons
D
RAB11
DAPI
TRKB
DAPI
TRKB
RAB11
DAPI
TRKB
RAB11
GFP
DAPI
TRKB colocalization with RAB11 (Mander's correlation coefficient)
0.5
0.4
0.3
0.2
0.1
0.0
***
WT Neurons
SORL1 OE Neurons
E
RAB11
DAPI
GLUA1
DAPI
GLUA1
RAB11
DAPI
GLUA1
RAB11
GFP
DAPI
GLUA1 colocalization with RAB11 (Mander's correlation coefficient)
0.5
0.4
0.3
0.2
0.1
0.0
*
WT Neurons
SORL1 OE Neurons

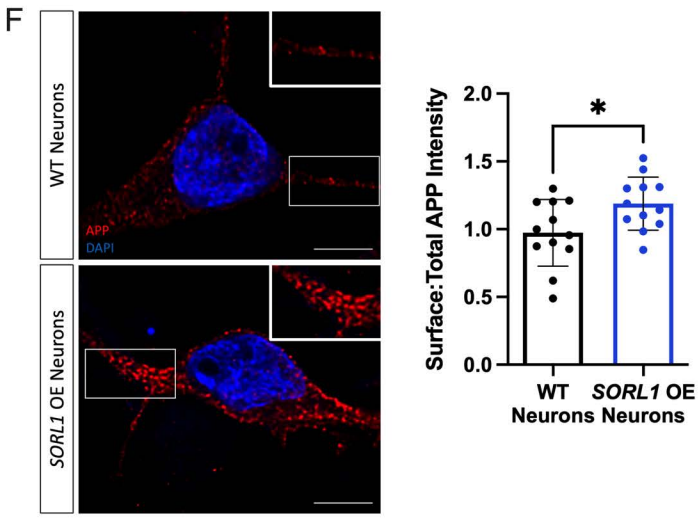
F
WT Neurons
SORL1 OE Neurons
APP
DAPI
Surface:Total APP Intensity
2.0
1.5
1.0
0.5
0.0
*
WT Neurons
SORL1 OE Neurons

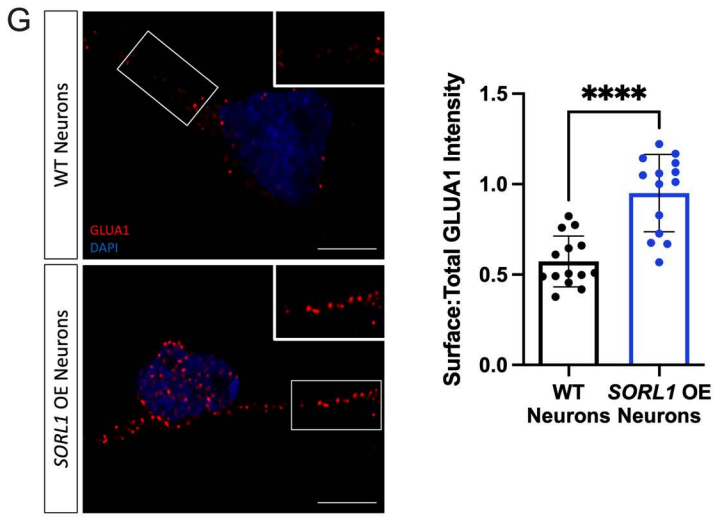
G
WT Neurons
SORL1 OE Neurons
GLUA1
DAPI
Surface:Total GLUA1 Intensity
1.5
1.0
0.5
0.0
****
WT Neurons
SORL1 OE Neurons

Figure 7

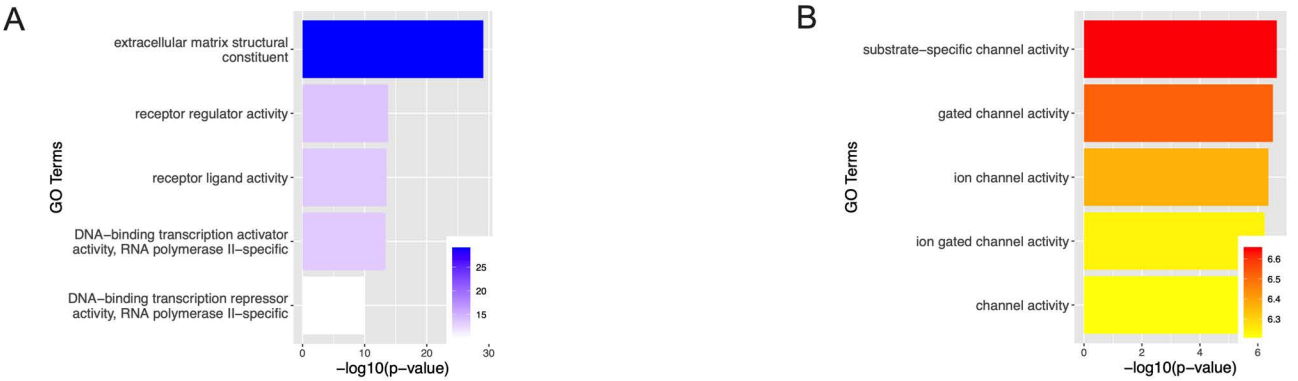
A
extracellular matrix structural constituent
receptor regulator activity
receptor ligand activity
DNA−binding transcription activator activity, RNA polymerase II−specific
DNA−binding transcription repressor activity, RNA polymerase II−specific
GO Terms
−log10(p−value)
B
substrate−specific channel activity
gated channel activity
ion channel activity
ion gated channel activity
channel activity
GO Terms
−log10(p−value)

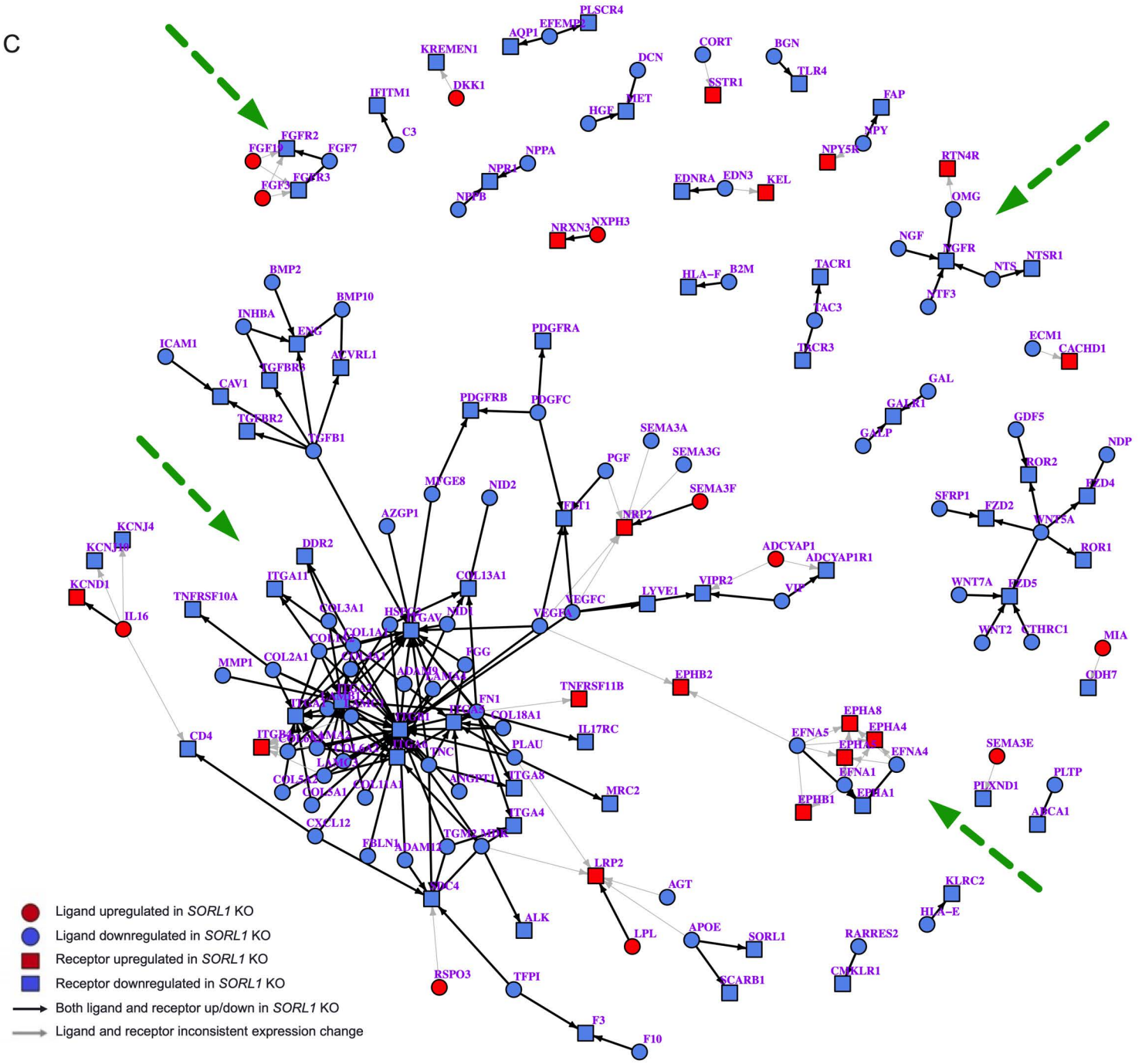
C
Ligand upregulated in SORL1 KO
Ligand downregulated in SORL1 KO
Receptor upregulated in SORL1 KO
Receptor downregulated in SORL1 KO
Both ligand and receptor up/down in SORL1 KO
Ligand and receptor inconsistent expression change

Figure 8

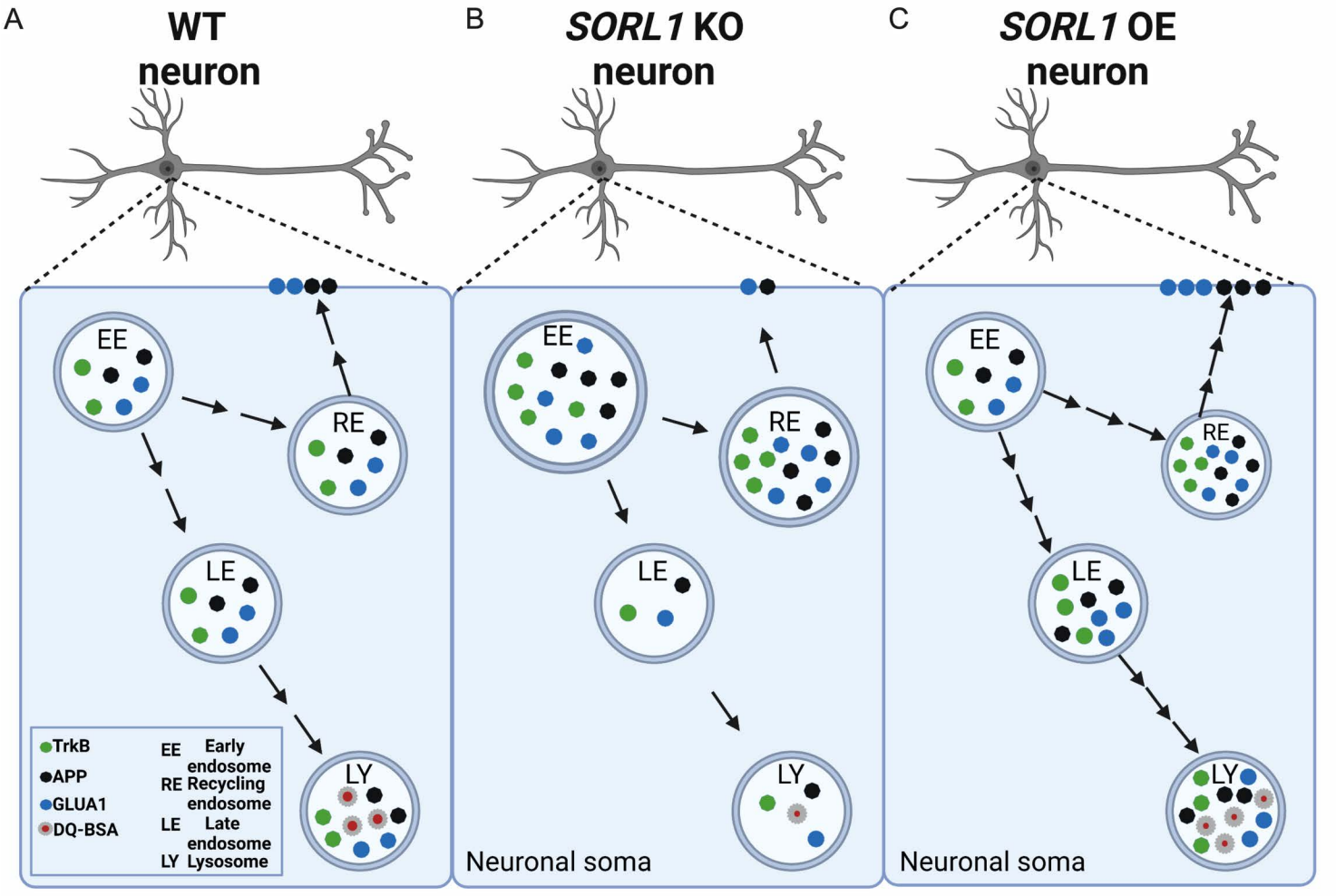
A
WT neuron
B
SORL1 KO neuron
C
SORL1 OE neuron
EE
RE
LE
LY
Neuronal soma
TrkB
APP
GLUA1
DQ-BSA
EE Early endosome
RE Recycling endosome
LE Late endosome
LY Lysosome

Supplemental Figure 1

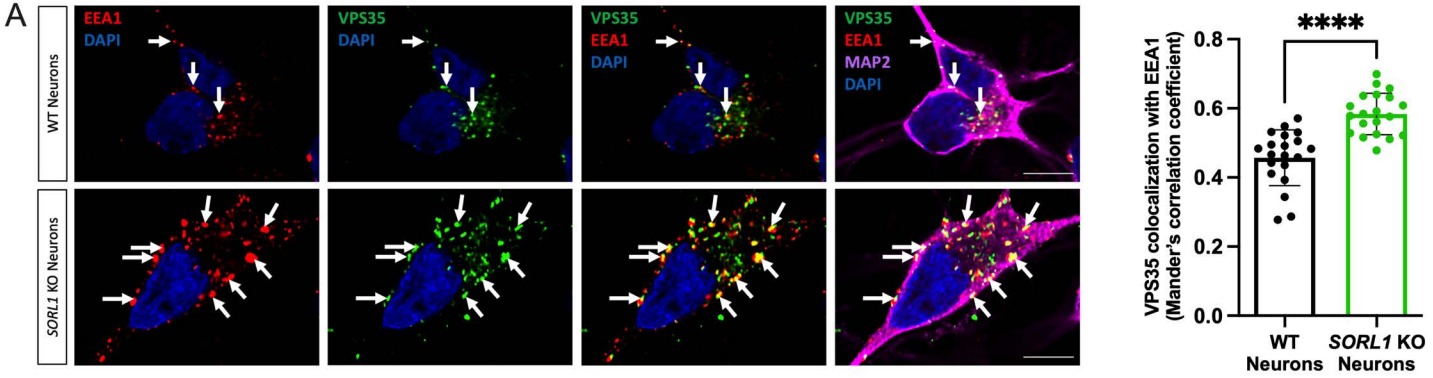

Supplemental Figure 2

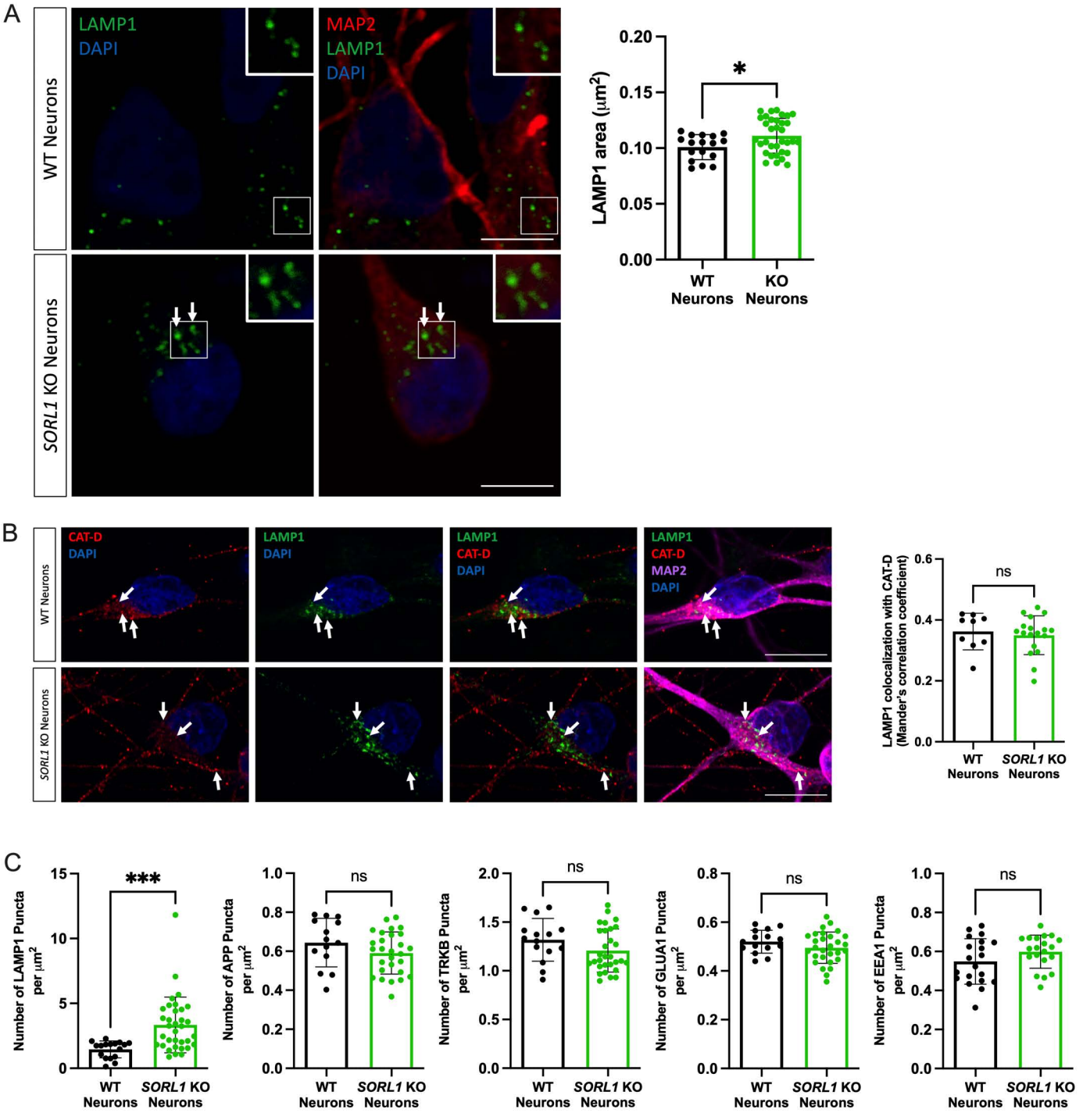

Supplemental Figure 3

A

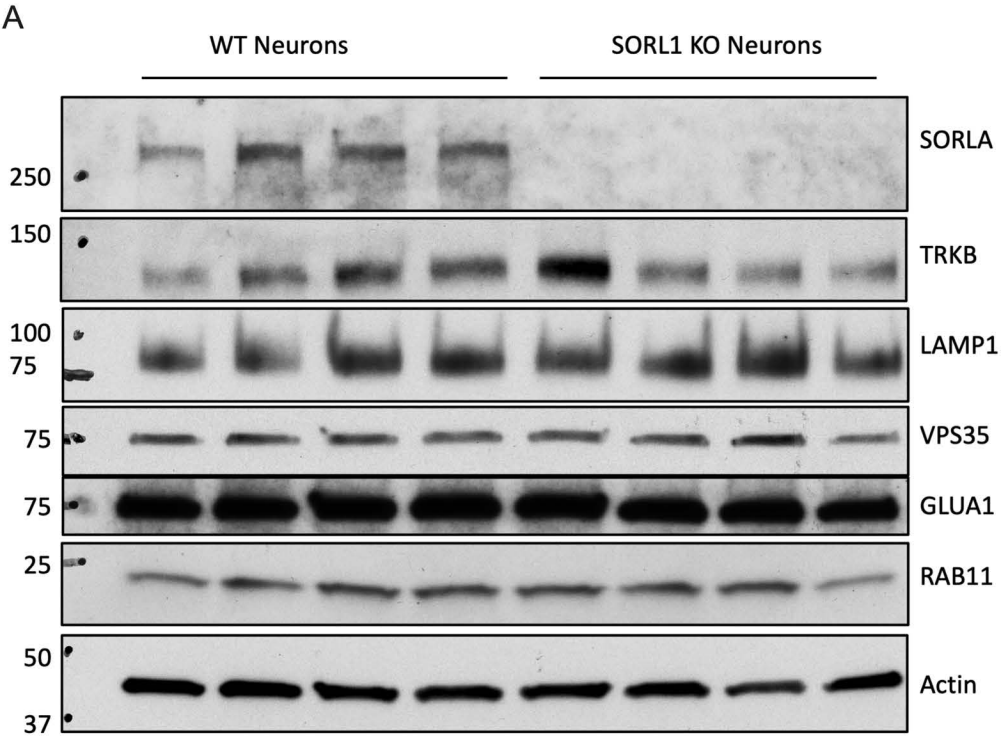


B

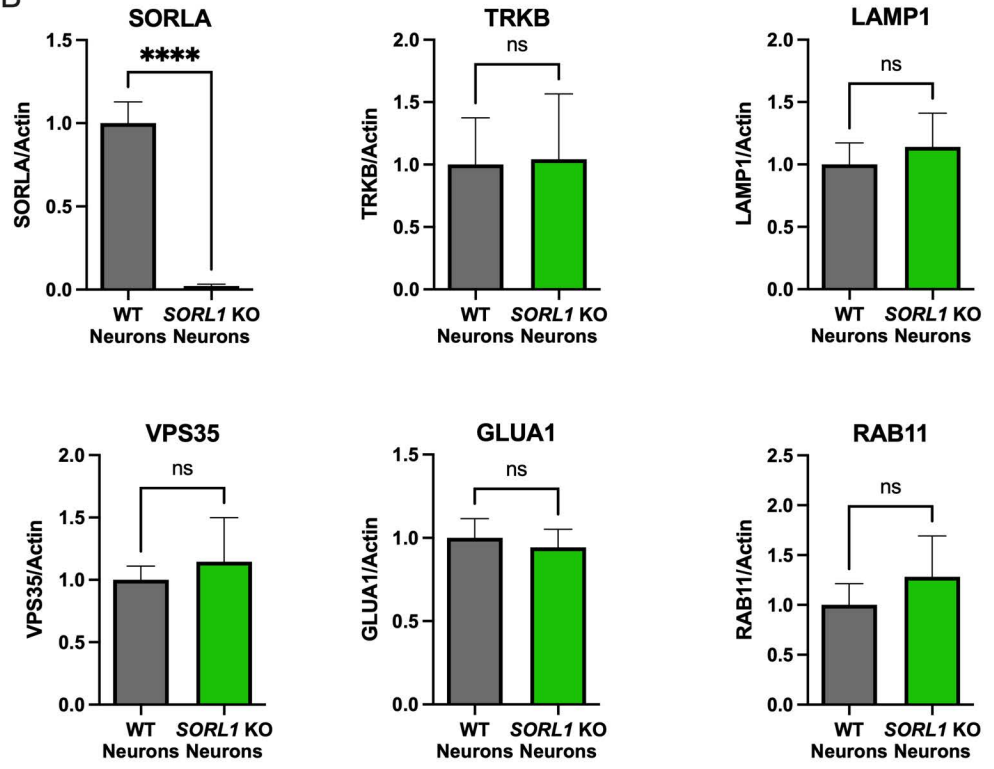

Supplemental Figure 4

A

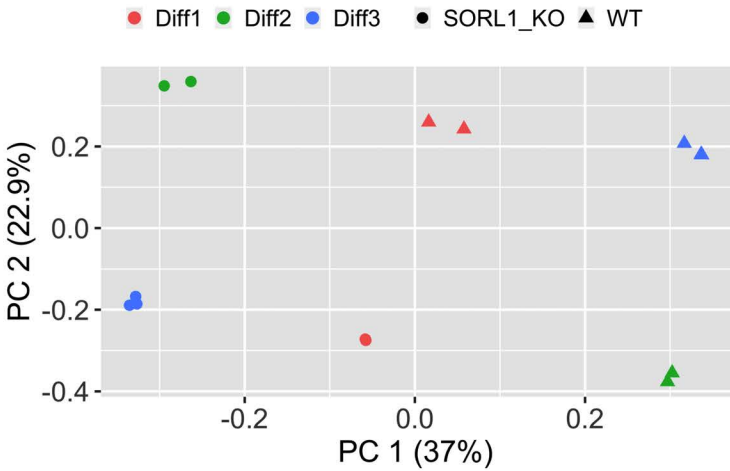


B

Significantly more downregulated than upregulated genes
p<2.2e-16

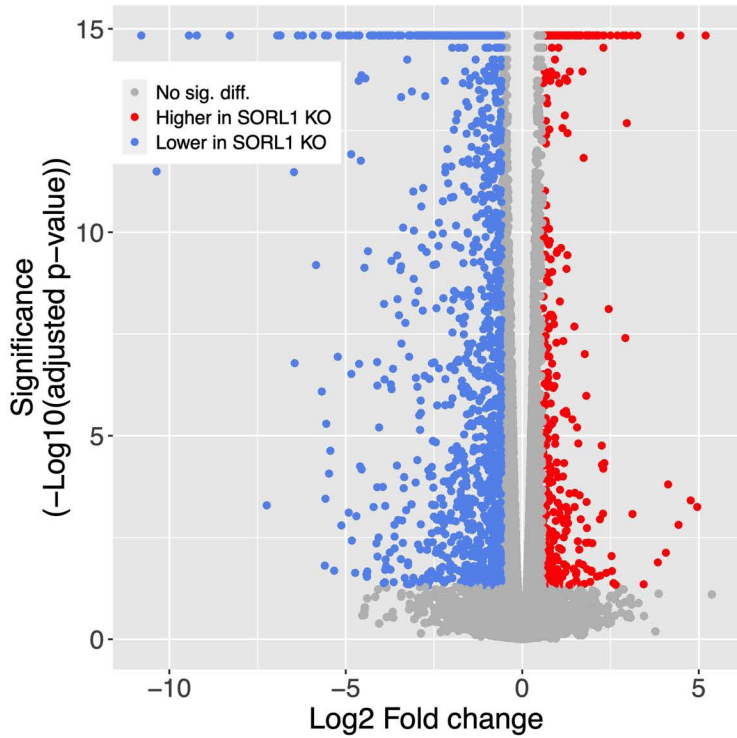

Supplemental Figure 5

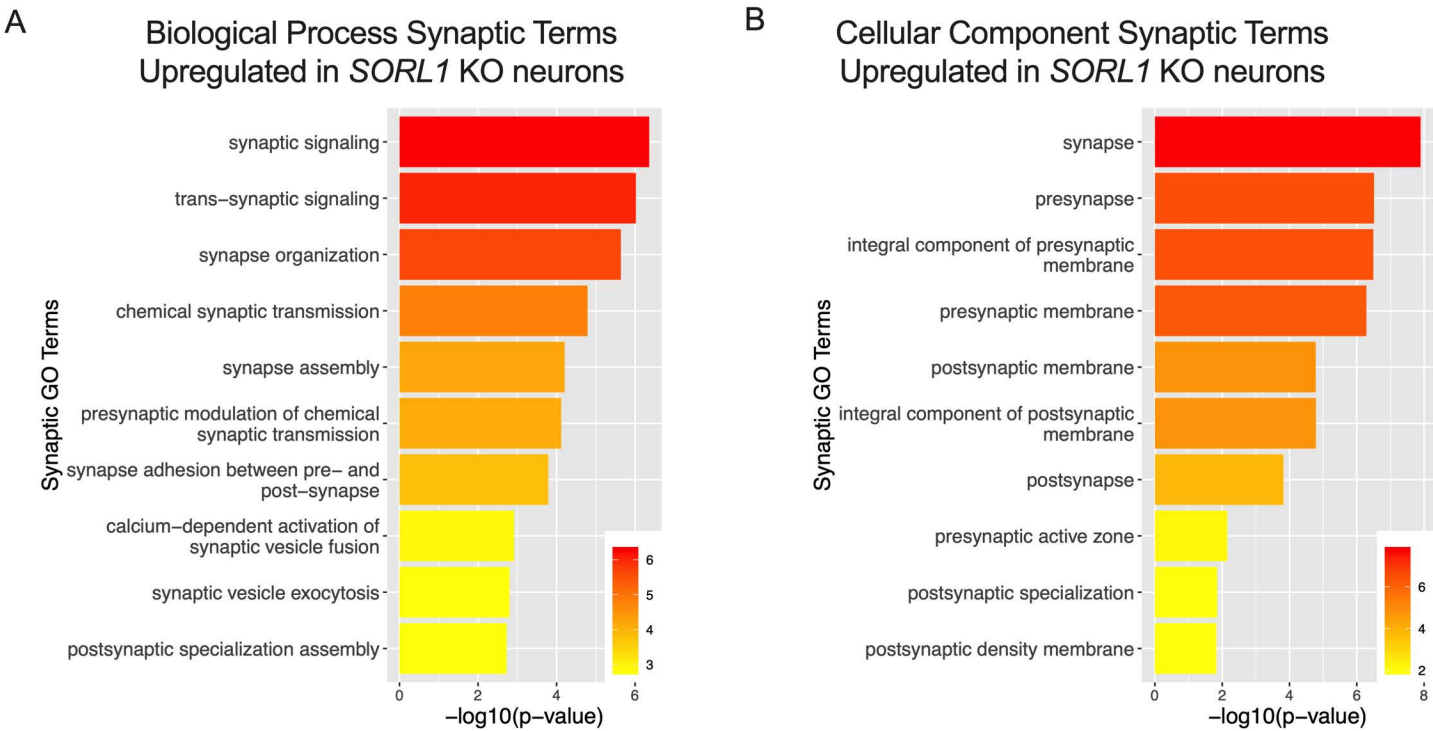

| Figure Number | Experimental Measure | Group A | Group B | Group A Mean | Group B Mean | Difference between means (B - A) ± SEM | 95% Confidence Interval |
|---|---|---|---|---|---|---|---|
| 1A | TRKB colocalization with EEA1 | WT Neurons | SORL1KO Neurons | 0.0799 | 0.1228 | 0.04290 ± 0.01042 | 0.02155 to 0.06425 |
| 1B | GLUA1 colocalization with EEA1 | WT Neurons | SORL1KO Neurons | 0.0496 | 0.1727 | 0.1231 ± 0.02257 | 0.07682 to 0.1693 |
| 2A | 6hr DQ Red BSA Intensity | WT Neurons | SORL1KO Neurons | 52.1 | 29.48 | -22.62 ± 2.684 | -28.09 to -17.15 |
| 2A | 24hr DQ Red BSA Intensity | WT Neurons | SORL1KO Neurons | 62.54 | 43.35 | -19.19 ± 3.608 | -26.58 to -11.80 |
| 2B | TRKB colocalization with RAB7 | WT Neurons | SORL1KO Neurons | 0.3102 | 0.2149 | -0.09530 ± 0.01234 | -0.1212 to -0.06937 |
| 2C | GLUA1 colocalization with RAB7 | WT Neurons | SORL1KO Neurons | 0.3828 | 0.286 | -0.09685 ± 0.02779 | -0.1538 to -0.03992 |
| 2D | APP colocalization with LAMP1 | WT Neurons | SORL1KO Neurons | 0.2983 | 0.1799 | -0.1184 ± 0.01951 | -0.1584 to -0.07844 |
| 2E | TRKB colocalization with LAMP1 | WT Neurons | SORL1KO Neurons | 0.071 | 0.04461 | -0.02639 ± 0.004876 | -0.03643 to -0.01635 |
| 2F | GLUA1 colocalization with LAMP1 | WT Neurons | SORL1KO Neurons | 0.1967 | 0.1588 | -0.03790 ± 0.02085 | -0.08060 to 0.004801 |
| 3A | 6hr DQ Red BSA Intensity | WT Neurons | SORL1OE Neurons | 30.31 | 27.84 | -2.473 ± 2.059 | -6.799 to 1.854 |
| 3A | 24hr DQ Red BSA Intensity | WT Neurons | SORL1OE Neurons | 32.61 | 39.73 | 7.123 ± 1.887 | 3.157 to 11.09 |
| 3B | APP colocalization with RAB7 | WT Neurons | SORL1OE Neurons | 0.7041 | 0.8008 | 0.09670 ± 0.02520 | 0.04375 to 0.1496 |
| 3C | TRKB colocalization with RAB7 | WT Neurons | SORL1OE Neurons | 0.44 | 0.5261 | 0.08610 ± 0.02417 | 0.03532 to 0.1369 |
| 3D | GLUA1 colocalization with RAB7 | WT Neurons | SORL1OE Neurons | 0.4287 | 0.5512 | 0.1225 ± 0.02485 | 0.07029 to 0.1747 |

| | | | | | | | |
|---|---|---|---|---|---|---|---|
| 3E | APP colocalization with LAMP1 | WT Neurons | SORL1OE Neurons | 0.1397 | 0.2949 | 0.1552 ± 0.02066 | 0.1118 to 0.1986 |
| 3F | TRKB colocalization with LAMP1 | WT Neurons | SORL1OE Neurons | 0.1539 | 0.2674 | 0.1135 ± 0.01501 | 0.08196 to 0.1450 |
| 3G | GLUA1 colocalization with LAMP1 | WT Neurons | SORL1OE Neurons | 0.1353 | 0.3206 | 0.1853 ± 0.02279 | 0.1374 to 0.2332 |
| 4A - T0 | Transferrin Intensity T0 | WT Neurons - T0 | SORL1KO Neurons - T0 | 100 | 100 | -4.167E-08 | -4.634 to 4.634 |
| 4A - T10 | Transferrin Intensity T10 | WT Neurons - T10 | SORL1KO Neurons - T10 | 64.14 | 82.82 | -18.68 | -24.35 to -13.00 |
| 4A - T20 | Transferrin Intensity T20 | WT Neurons - T20 | SORL1KO Neurons - T20 | 58.44 | 67.48 | -9.038 | -13.67 to -4.404 |
| 4A - T40 | Transferrin Intensity T40 | WT Neurons - T40 | SORL1KO Neurons - T40 | 56.41 | 68.96 | -12.55 | -17.19 to -7.920 |
| 4B | Rab11 Area | WT Neurons | SORL1KO Neurons | 0.06625 | 0.073 | 0.006747 ± 0.002882 | 0.0009338 to 0.01256 |
| 4C | APP colocalization with RAB11 | WT Neurons | SORL1KO Neurons | 0.2689 | 0.3147 | 0.04580 ± 0.01442 | 0.01626 to 0.07534 |
| 4D | TRKB colocalization with RAB11 | WT Neurons | SORL1KO Neurons | 0.1071 | 0.2277 | 0.1206 ± 0.02924 | 0.06071 to 0.1805 |
| 4E | GLUA1 colocalization with RAB11 | WT Neurons | SORL1KO Neurons | 0.2605 | 0.3065 | 0.04595 ± 0.01599 | 0.01320 to 0.07870 |
| 5A | Surface:Total APP Intensity | WT Neurons | SORL1KO Neurons | 1.128 | 0.5124 | -0.6157 ± 0.05825 | -0.7331 to -0.4982 |
| 5B | Surface:Total GLUA1 Intensity | WT Neurons | SORL1KO Neurons | 1.022 | 0.5769 | -0.4451 ± 0.04588 | -0.5368 to -0.3534 |
| 5C | D27 Weighted Mean Firing | WT Neurons | SORL1KO Neurons | 3.768 | 7.696 | 3.928 ± 1.266 | 1.169 to 6.687 |
| 5C | D66 Weighted Mean Firing | WT Neurons | SORL1KO Neurons | 7.074 | 3.784 | -3.289 ± 1.101 | -5.688 to -0.8903 |

| | | | | | | | |
|---|---|---|---|---|---|---|---|
| 6A - T0 | Transferrin Intensity T0 | WT Neurons - T0 | SORL1OE Neurons - T0 | 100 | 100 | -0.0000002 | -11.47 to 11.47 |
| 6A - T10 | Transferrin Intensity T10 | WT Neurons - T10 | SORL1OE Neurons - T10 | 82.52 | 69.57 | 12.95 | 1.483 to 24.42 |
| 6A - T20 | Transferrin Intensity T20 | WT Neurons - T20 | SORL1OE Neurons - T20 | 74.47 | 59.35 | 15.12 | 3.653 to 26.59 |
| 6A - T40 | Transferrin Intensity T40 | WT Neurons - T40 | SORL1OE Neurons - T40 | 68.31 | 55.43 | 12.89 | 1.419 to 24.35 |
| 6B | Rab11 Area | WT Neurons | SORL1OE Neurons | 0.101 | 0.09005 | -0.01099 ± 0.003199 | -0.01742 to -0.004558 |
| 6C | APP colocalization with RAB11 | WT Neurons | SORL1OE Neurons | 0.3903 | 0.5878 | 0.1975 ± 0.02717 | 0.1404 to 0.2546 |
| 6D | TRKB colocalization with RAB11 | WT Neurons | SORL1OE Neurons | 0.1846 | 0.2969 | 0.1123 ± 0.02416 | 0.06155 to 0.1631 |
| 6E | GLUA1 colocalization with RAB11 | WT Neurons | SORL1OE Neurons | 0.2509 | 0.2965 | 0.04560 ± 0.01822 | 0.007315 to 0.08389 |
| 6F | Surface:Total APP Intensity | WT Neurons | SORL1OE Neurons | 0.9734 | 1.189 | 0.2155 ± 0.09083 | 0.02710 to 0.4038 |
| 6G | Surface:Total GLUA1 Intensity | WT Neurons | SORL1OE Neurons | 0.5727 | 0.9505 | 0.3778 ± 0.06831 | 0.2374 to 0.5182 |
| Supplementary 1A | VPS35 colocalization with EEA1 | WT Neurons | SORL1KO Neurons | 0.457 | 0.5838 | 0.1268 ± 0.02249 | 0.08129 to 0.1724 |
| Supplementary 2A | LAMP1 area | WT Neurons | SORL1KO Neurons | 0.1008 | 0.1112 | 0.01032 ± 0.004276 | 0.001730 to 0.01892 |
| Supplementary 2B | Cathepsin-D colocalization with LAMP1 | WT Neurons | SORL1KO Neurons | 0.3621 | 0.3499 | -0.01219 ± 0.02558 | -0.06488 to 0.04051 |
| Supplementary 2C | Number of LAMP1 puncta per $\mu m^2$ | WT Neurons | SORL1KO Neurons | 1.452 | 3.339 | 1.887 ± 0.5339 | 0.8145 to 2.960 |
| Supplementary 2C | Number of APP puncta per $\mu m^2$ | WT Neurons | SORL1KO Neurons | 0.6442 | 0.5906 | -0.05352 ± 0.03725 | -0.1288 to 0.02175 |

| | | | | | | | |
|---|---|---|---|---|---|---|---|
| Supplementary 2C | Number of TRKB puncta per $\mu m^2$ | WT Neurons | SORL1KO Neurons | 1.318 | 1.208 | -0.1100 ± 0.06986 | -0.2509 to 0.03084 |
| Supplementary 2C | Number of GLUA1 puncta per $\mu m^2$ | WT Neurons | SORL1KO Neurons | 0.5202 | 0.4951 | -0.02509 ± 0.01880 | -0.06303 to 0.01285 |
| Supplementary 2C | Number of EEA1 puncta per $\mu m^2$ | WT Neurons | SORL1KO Neurons | 0.5488 | 0.5986 | 0.04975 ± 0.03228 | -0.01560 to 0.1151 |
| Supplementary 3B | SORLA/Actin | WT Neurons | SORL1KO Neurons | 1 | 0.02221 | -0.9778 ± 0.06426 | -1.135 to -0.8205 |
| Supplementary 3B | TRKB/Actin | WT Neurons | SORL1KO Neurons | 1 | 1.043 | 0.04315 ± 0.3219 | -0.7444 to 0.8307 |
| Supplementary 3B | LAMP1/Actin | WT Neurons | SORL1KO Neurons | 1 | 1.141 | 0.1413 ± 0.1599 | -0.2499 to 0.5324 |
| Supplementary 3B | VPS35/Actin | WT Neurons | SORL1KO Neurons | 1 | 1.146 | 0.1459 ± 0.1848 | -0.3064 to 0.5982 |
| Supplementary 3B | GLUA1/Actin | WT Neurons | SORL1KO Neurons | 1 | 0.9428 | -0.05717 ± 0.07946 | -0.2516 to 0.1373 |

Supplemental Table 1.